BIOCYBERNETIC FAB FACTORS IN HUMAN PERCEPTION AND MEMORY

David C. Lai

Stanford University

Prepared for:

Advanced Research Projects Agency

July 1974

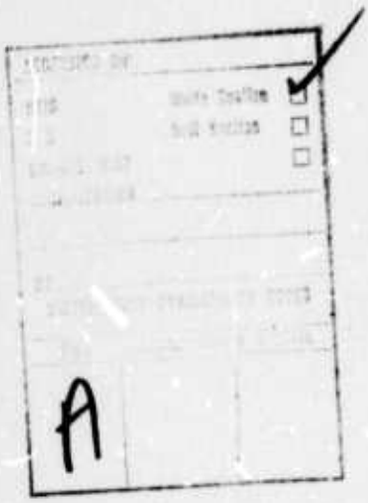

The views and conclusions contained in this document are those of the authors and should not be interpreted as necessarily representing the official policies, either expressed or implied, of the Advanced Research Projects Agency or the U. S. Government.

SEL-74-034

ANNUAL REPORT

for the Advanced Research Projects Agency

of the Department of Defense

BIOCYBERNETIC FACTORS IN HUMAN PERCEPTION AND MEMORY

PRINCIPAL INVESTIGATOR:

Dr. David C. Lai

Contract No. DAHC15-72-C-0232

ARPA Order No. 2190

July 1974

Technical Report No. 6741-3

1 June 1973 to 31 May 1974

Department of Electrical Engineering
Stanford Electronics Laboratories
Stanford University Stanford, California 94305

PROFESSIONAL PERSONNEL

Dr. D. C. Lai, Visiting Professor of Electrical Engineering, Principal Investigator

Dr. T. Kailath, Professor of Electrical Engineering, Co-Principal Investigator

Dr. H. S. Magnuski, Post-doctoral Research Fellow

Dr. J. E. Anliker, Consultant

K. H. Jacker (B.A. in Computer Science and B.A. in Mathematics), Scientific Programmer

A. Huang (M.S.E.E.), Scientific Programmer

A. Shah (M.S.E.E.), Graduate Student Research Assistant

M. Stauffer (M.S.E.E.), Graduate Student Research Assistant

J. Nickolls (M.S.E.E.), Graduate Student Research Assistant

R. Floyd (M.S.E.E.), Graduate Student Research Assistant

FOREWORD

This annual technical report presents the accomplishments during the period of 1 June 1973 to 31 May 1974. The principal investigator is Dr. D. C. Lai and co-principal investigator is Dr. T. Kailath. Since the inception of this project, it has been the result of the collaborative efforts of many individuals. In particular, Dr. J. E. Anliker has spent endless hours on this project. Most of the staff members contributed in the writing of this report.

Biocybernetic Factors in Human Perception and Memory

SUMMARY

This project is concerned with the application of biocybernetic concepts to the problem of expanding human memory. In particular, the goal of this research is enhancement of visual imagery as far as possible in the direction of photographic memory. Scanpaths of the eye during inspection of visual targets are treated as indicators of the brain's strategy for the intake of visual information. This research will determine the features that differentiate scanpaths associated with superior imagery from scanpaths associated with inferior imagery. Similarly, the tachistoscopic exposure of the visual material is responsible for a number of adjustments in the brain's waking rhythm; the electroencephalographic features correlated with superior imagery will be differentiated from those correlated with inferior imagery. A computerized biocybernetic scheme will be implemented in an attempt to generate image enhancement and to train the individual to exert greater voluntary control over his own imagery. In this technical report, we give an account of our accomplishments made in this reporting period.

We made significant progress in eye-movement measurement and tracking during the past year. New techniques for eye-movement prediction and special software for visual scanpaths study have been developed and implemented. A real-time scanpath analysis program has been implemented. Progress has been made in the determination of features that differentiate scanpaths associated with superior imagery from those associated with inferior imagery through the use of a new experiment paradigm and various

scanpath analysis schemes. In the direction towards discovering the temporal cues that serve as the keys for visual memory encoding and retrieval, we made a study of the visual evoked response (VER) contingent upon the phases of EEG at which the photic stimuli were delivered. We also describe an EEG signal model which prescribes the stimulus-response relationship. The information gained in this model will elucidate the behavior of the alpha frequency and phase, and thus lead to a more practical brain state estimator and predictor for our use in the memory studies of this project.

During this reporting period, we published and presented six papers at various international and national scientific conferences in addition to papers published in the first contract year, and one paper has been submitted and accepted for presentation at the forthcoming Conference on Engineering in Medicine and Biology.

This research project has significant implications for the Department of Defense since the research results obtained enhance the potential for devising new and unusual techniques that will permit the development of stronger imagery in men with normal memories. Because it is definitely an asset for the military man to have the ability to absorb information rapidly and to retain it intact for long period of time, this project will attempt to intensify the post-stimulus imagery as far as possible in the direction of photographic memory--and to search out those features of successful recall strategies so as to enhance the individual's power of redintegration.

TABLE OF CONTENTS

LIST OF FIGURES

I. INTRODUCTION

The objective of this research project is to develop biocybernetic concepts and techniques useful for the analysis and development of skills required for the enhancement of the concrete images of the "eidetic" type. In particular, we are concentrating on the problem of achieving biocybernetic expansion of human visual memory through the use of a closely-coupled man-machine system which performs real-time monitoring and feedback of cues that serve as keys to memory encoding and retrieval. This approach is based on the considerable evidence that the human nervous system depends heavily upon spatial and temporal cues both in the encoding and decoding of memories, especially sensory images. One of the principal limiting factors in the design of closely-coupled man-machine systems is our limited knowledge of human memory mechanisms. We believe that closely-coupled man-machine systems can be used not only for the measurement and prediction of human mnemonic performance, but also for the control and enhancement of human mnemonic skills.

Our scheme is to develop and implement techniques for real-time monitoring and prediction of central nervous activities through the analysis of eye movements and EEG signals. We have made significant progress in the development and implementation of these monitoring techniques. The information obtained in the monitoring and analysis of the cortical activities is being used to arrange extraordinary coincidences between eye pointing, brain states, and the control of stimulus patterns using optimal feedback control schemes. The visual stimuli are presented in various ways (projection screen, oscilloscopic displays, or in complex tachistoscopic batteries) for either monopic or dichopic viewing. The

optical and electrophysiological estimators are obtained by measuring the eye position and eye movements through a unified system. By combining these techniques and using various feedback schemes to close the control loop thereby forming a closely coupled man-machine system, we are attempting to achieve greater control of image persistence and image dissipation. Our design of such a closely-coupled man-machine system is depicted in Figure I.1. We utilize computer-based models in our system configuration to predict (forward-time analysis) the kind of stimuli which should be used in order to produce the desired future responses. The EEG signal and the eye-movement measurement are shown as the responses which are closely controlled since the models are designed to mimic the actual physiological processes in regard to their stimulus-response relations. The boxes in the block diagram of Figure I.1 are labeled according to their functions. All except the interface electronic systems are to be implemented on the PDP-15 computer, which is the heart of the implementation of our schemes. Our work has been progressing in the direction of achieving the realization of this closely-coupled man-machine system. We have designed and implemented some of the interface electronic systems and signal processing algorithms. Real-time estimation and prediction algorithms for monitoring brain states and eye pointing are being designed. The development of some modeling schemes for eye movements and EEG signals is in progress. In this report, we present our accomplishments in developing and implementing those concepts and schemes which are essential for the realization of our closely-coupled man-machine system for visual memory enhancement.

In the past contract year, our major effort was devoted to eye-

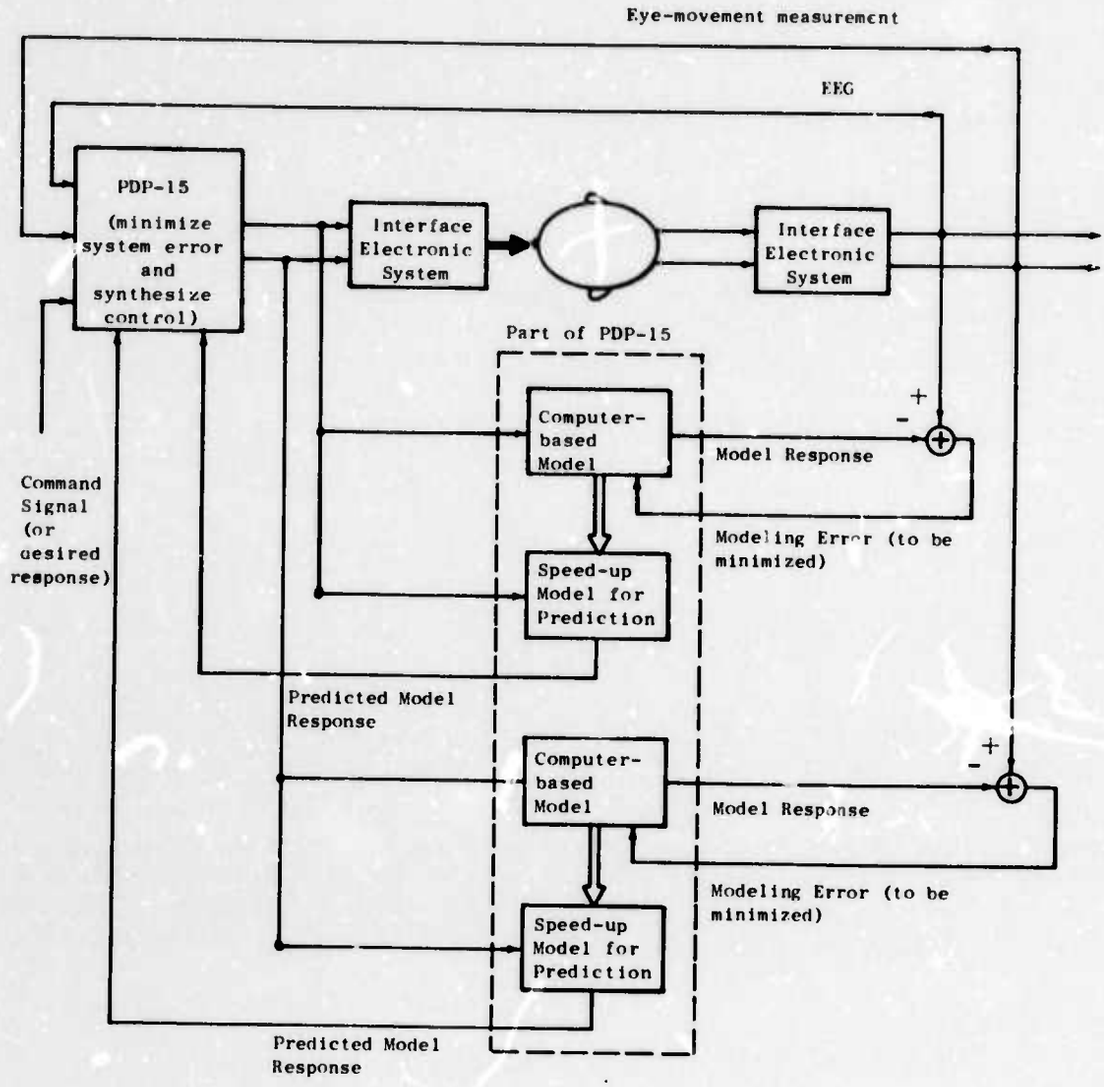

Figure I.1 Block diagram of the closely-coupled man-machine system for visual memory tracking and training.

movement measurement and tracking and the scanpath study for the determination of spatial cues that serve as keys to memory encoding and retrieval. Progress has also been made in the determination of the temporal cues which are thought to be useful for memory encoding and recall.

A phase contingent analysis of visual evoked responses has been made. This study shows that there is a definite excitability cycle correlated with the phase of the alpha rhythm at the instant of photic stimulation. This will be described in Section VII. In the next section, we describe new calibration procedures and distortion-correcting schemes for our Biometrics eye-movement monitor. This improves the accuracy of our eye-movement data; however, we have exploited the full capability of the Biometrics eye-movement monitor system. We foresee that more accurate eye-movement data are needed in our future work. In Section III, we present our progress in developing new techniques for eye-movement monitoring and tracking. In order to study the visual scanpaths associated with superior (eidetic) imagery and those associated with ordinary imagery as to discover the spatial features that are more memorable, we devised a new experiment paradigm. Its methods and the preliminary analysis of the scanpath data are presented in Section IV. Since an effective real-time scanpath analysis is essential for implementing cybernetic models for the prediction and feedback of ongoing eye-pointing behavior, we have developed and realized such a real-time scanpath analyzer. This is described in Section V. In Section VI, we present an EEG signal model that relates the photic stimuli and the EEG signal and some new results. The understanding of this stimulus-response relationship is essential in the determination of the temporal cues that play prominent roles in the encoding and decoding of visual memory. As mentioned previously, we describe the phase contingent averages of visual evoked responses in Section VII. Some concluding remarks and future work are described in the last section.

II. CALIBRATION AND DISTORTION CORRECTION OF EYE-MOVEMENT MEASUREMENT

In searching for the spatial and temporal cues that serve as keys to encoding and recall of visual memory, we need an accurate technique for the measurement of eye movement and eye position. At present, we are using the Eye-Movement Monitor (Type SG) manufactured by Biometrics, Inc. This instrument provides a simple and relatively easy-to-use method for measurement of horizontal and vertical movements of the eye. In the horizontal direction, the method is based on the measurement of the amount of infra-red light reflected from the junction of the iris and the sclera. In the vertical direction, the eyelid-sclera junction is used. The signal produced is not linear and is susceptible to several sources of noise which affect both the reproducibility and quality of the measurements. The major sources of difficulties are:

(1) Movement of the head or the spectacles on which the sensors are mounted results in translation of the X,Y coordinate space.

(2) Cross-talk between X and Y measurements; i.e., horizontal eye-movements influence "vertical" output voltages, and vice versa.

(3) The vertical signal suffers from an "eyelid hysteresis" phenomenon; that is, the eyelid does not always return to exactly the same position near the corneo-scleral junction after vertical movement or blinks.

(4) Nonlinearities are introduced in both X and Y signals due to changes in the adjustment of the apparatus and through differences in the characteristics of the eyes of the subjects.

Consequently, we are confronted with the problem of trying to compensate

for the noises and nonlinearities in the eye monitor. The response characteristics of the eye-sensor system can be represented by curves similar to the ones shown in Figure II.1 where only the horizontal response curve is shown. Given the output (voltages from the Biometrics) we are trying to find ways of estimating the true input (eye position).

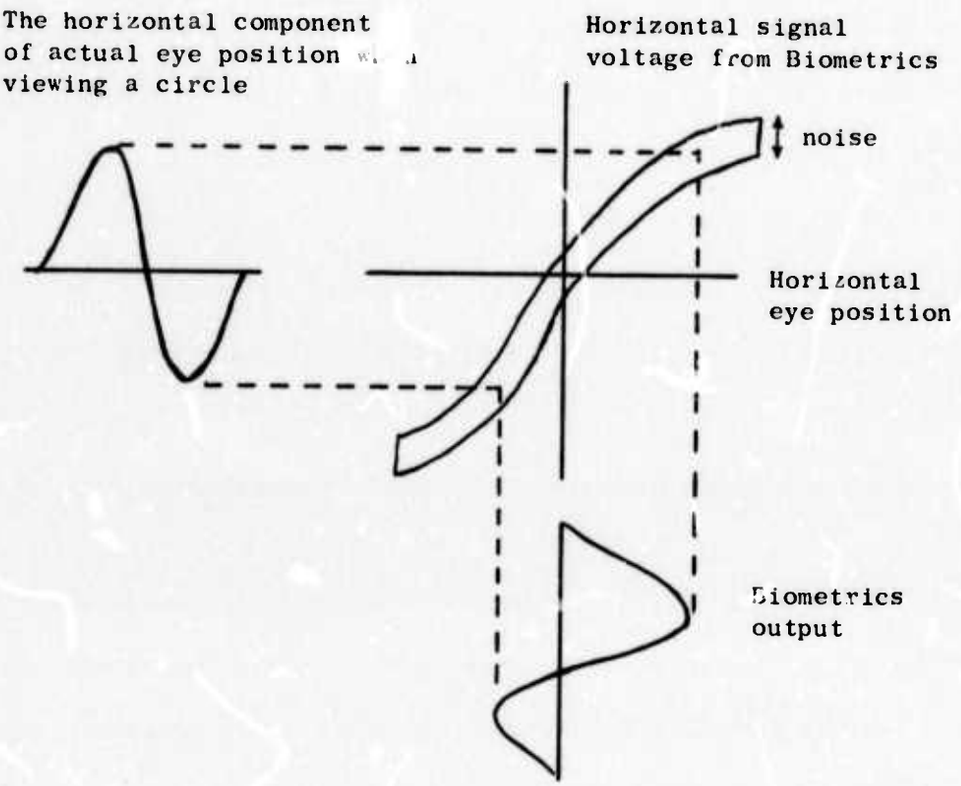

Figure II.1 Horizontal response curve
for eye-sensor system.

We are using two main approaches to the problem of compensating for nonlinearities. One is to model the response curve via piecewise linearization techniques; that is, we attempt to linearize the nonlinear X and Y voltages to match the linear space of the visual stimulus. The other approach is to translate the linear features of the visual stimulus into the nonlinear domain of the eye tracker and thus achieve

a closer match between stimulus and response.

In the case of piecewise linearization, we let (r_1, r_s) represent the measured X,Y voltage values corresponding to some stimulus point (s_1, s_2), then the most general form of a linear mapping between r and s is of the form

$$s_1 = c_{11} r_1 + c_{12} r_2 + c_{13}$$

$$s_2 = c_{21} r_1 + c_{22} r_2 + c_{23} \quad .$$

The coefficients c_{ij} are defined by use of a three point calibration array which empirically determines the relationship between the stimulus values (s_1, s_2) and the response values (r_1, r_2).

Measured value		Stimulus value
(r_{1a}, r_{2a})	corresponds to	(s_{1a}, s_{2a})
(r_{1b}, r_{2b})	corresponds to	(s_{1b}, s_{2b})
(r_{1c}, r_{2c})	corresponds to	(s_{1c}, s_{2c})

This correspondence allows us to set up two sets of three simultaneous linear equations, the first of which is

$$s_{1a} = c_{11} r_{1a} + c_{12} r_{2a} + c_{13}$$

$$s_{1b} = c_{11} r_{1b} + c_{12} r_{2b} + c_{13}$$

$$s_{1c} = c_{11} r_{1c} + c_{12} r_{2c} + c_{13} \quad .$$

Solution of these equations yields the required coefficients.

In practice, one such linear mapping is not sufficient to correct for distortions introduced by the Biometrics unit. The problem, in general, is to find the minimum number of stimulus calibration points (and thus the number of mappings) needed to reduce the nonlinear distortion to a level below the other noise sources mentioned above.

A program has been written which computes the c_{ij} coefficients

for the mappings. It consists of two subroutine calls named MAPSET and MAPCNV. The visual field is divided into three to eight pie-shaped sectors around a pivot point in the center of the visual field. A set of coefficients is computed for each sector by MAPSET. The second routine, MAPCNV, determines which sector applies to a given measured point (r_1, r_2) and computes the corresponding stimulus value (s_1, s_2).

The program IBALL, originally developed to gather statistical data about the response curve, was modified to incorporate this piecewise linearization technique. The program basically presents various points distributed over the visual space on a storage scope to a subject These points are repeated a point-at-a-time in a random sequence. The responses from the Biometrics unit are recorded by the computer. The statistical properties of the responses corresponding to each of the various points are then computed. Figure II.2 shows the results of one such experiment. The circles show the points which were presented to the subject. In this case each point was presented ten times in the course of the experiment. The cluster of spots about these circles indicate the actual measured responses. The crosses represent the statistical properties of the individual clusters. The lengths of the horizontal and vertical bars are proportional to the standard deviation of the error in each of the corresponding directions. It is seen that the responses are distorted by the nonlinearities and vertical crosstalk. As a demonstration of the capabilities of piecewise linearization, the means of each of the distorted clusters were used to form the response matrix for MAPSET while the coordinates of the actual stimulus points determine the stimulus array. The measurements recorded via the Biometrics were then remapped by MAPCNV and displayed as shown in Figure II.3. Figures II.4 and II.5 show the

correction of badly distored cases.

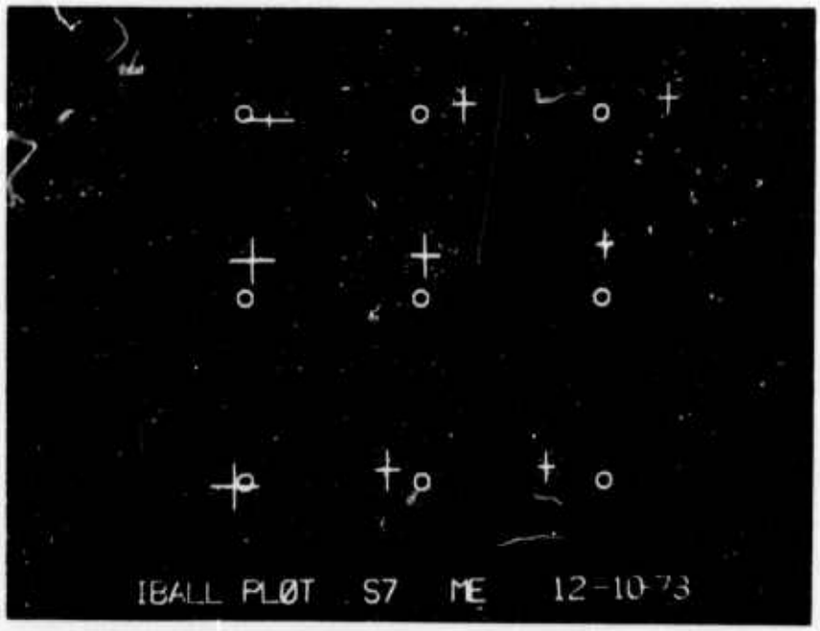

Figure II.2 Average display of IBALL of Subject 7

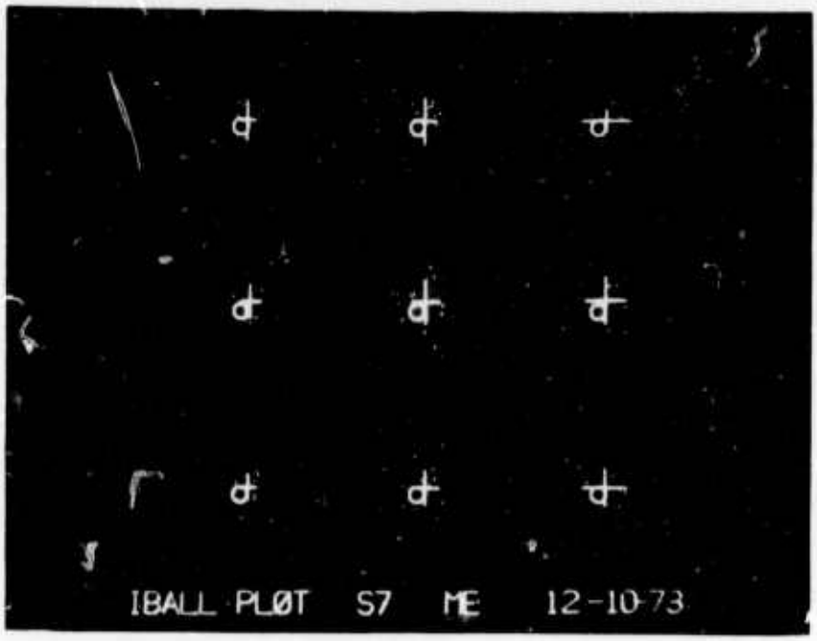

Figure II.3 Skew removed from S7

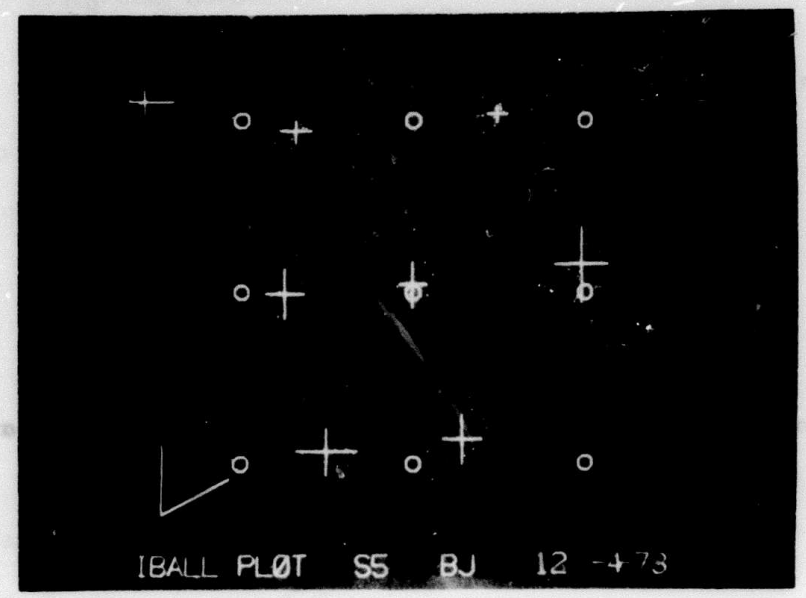

Figure II.4 Highly distorted before correction

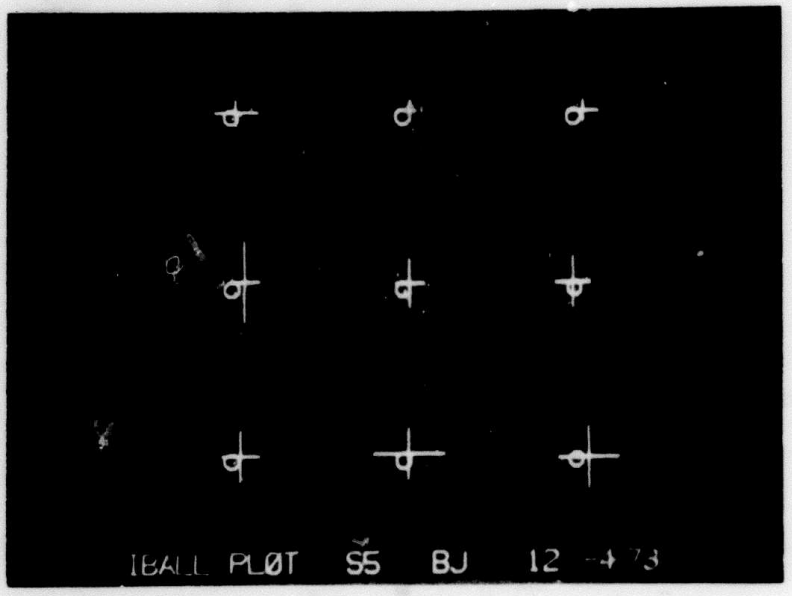

Figure II.5 Distortion corrected

It is seen that the piecewise linearization method is limited to the correction of small distortions. The amount of distortion is, in turn affected by the noise in the environment. The variations in the response curve for the horizontal response have been measured to range from .4 to 1.2 degrees of visual angle and those for vertical response were about twice the horizontal range.

Another means of compensating for nonlinearities in the eye monitor is to translate the outline of the stimulus into the nonlinear domain of the eye monitor by having the subject trace a cartoon of the linear stimulus relating actual eye position to output signal. The general approach is schematically shown in Figure II.6 A subject is shown a

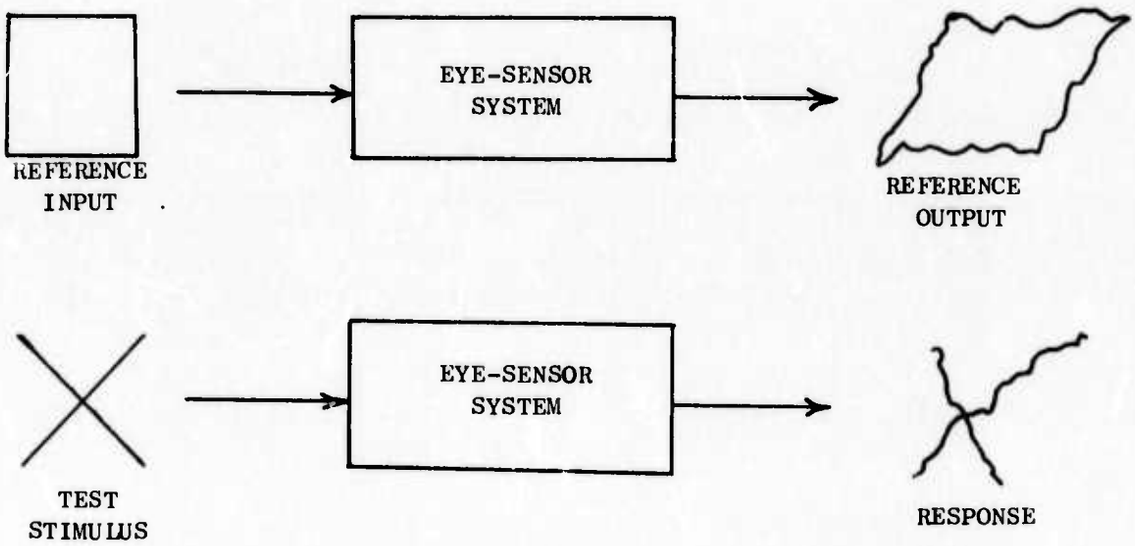

Figure II.6 Compensation of nonlinearity by nonlinear means.

stimulus (say, a square) on the storage scope. His scanpath response is then recorded. The subject is also required to track a spot of light that moves along the stimulus cartoon stored in the SEER program. In this way, the nonlinear scanpath can be compared with a similarly nonlinear version of the stimulus cartoon and thereby achieve a closer

match between scanpath fixations and stimulus features.

The line drawing (linear) which was used as the visual stimulus shown in Figure II.7 was drawn on the storage scope and briefly presented to the observer. His eye movements were measured by the Biometrics unit while he was free-viewing the scene. He was then asked to slowly trace the scene by following a moving light spot generated by SEER. The scanpath is superimposed on the non-linear tracing in Figure II.8; compare this with the same scanpath superimposed on the original linear stimulus shown in Figure II.9

Figure II.7 Line drawing
used for visual stimulus

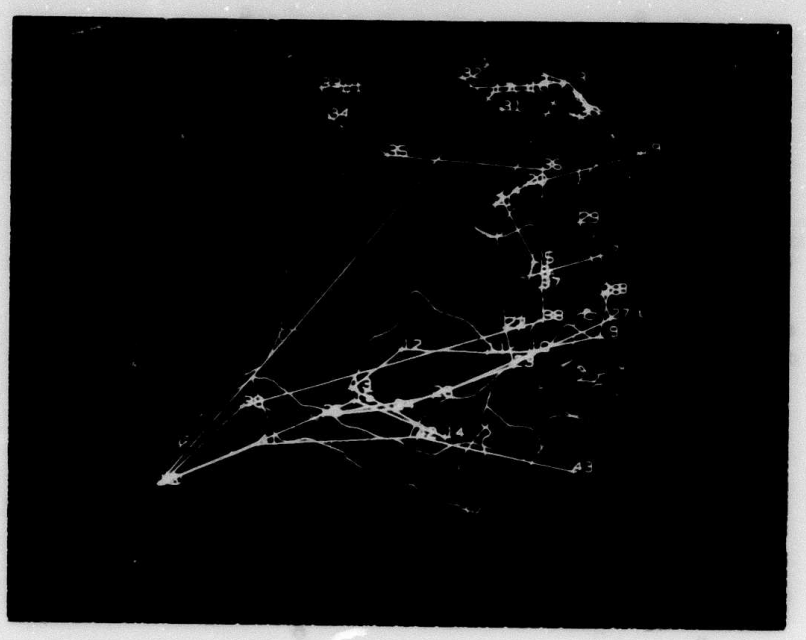

Figure II.8 Scanpath superimposed on the nonlinear tracing.

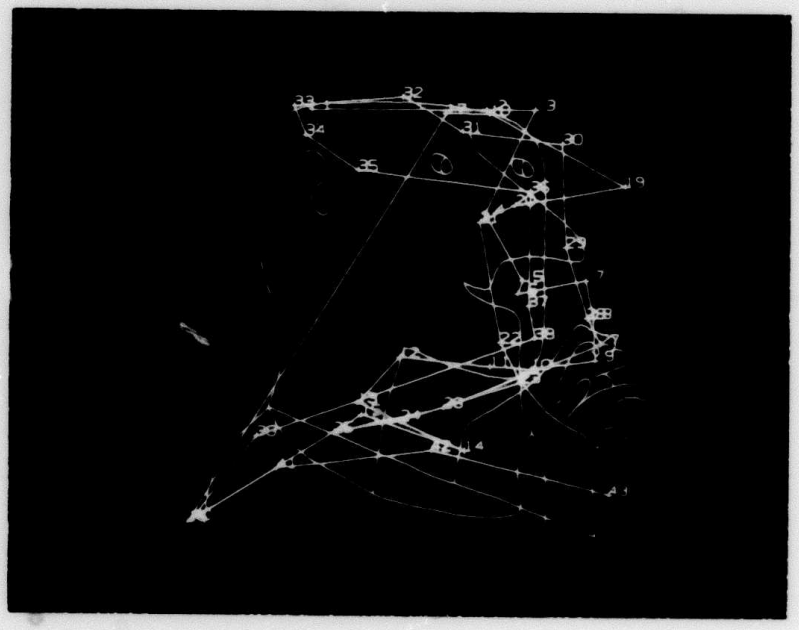

Figure II.9 Scanpath superimposed on the original drawing.

III. EYE-MOVEMENT MONITORING AND TRACKING

1. Introduction

The tracking of eye movement is an essential part of our research project. In order to feedback the spatial cues in encoding and decoding of memories, we have to track constantly the movement of the eyes. Basically, for the kind of eye movements we are interested in, we can classify them into two modes; viz., fixation and saccades. Thus, for the purpose of monitoring and tracking we need to (a) estimate and predict the duration of a fixation when in that mode; i.e., to predict when the mode will change from a fixation to a saccade and (b) estimate and predict the duration, the direction, and the length of the saccade for the saccadic movement itself, i.e., to predict when and where the saccade will end.

The two parts are interdependent. Ultimately, we will build a model which will take care of both. However, more insight can be obtained if we deal with the two separately and then combine them into one predictive model. At present, we have looked into part (b). For the sake of simplicity, we will first develop a deterministic model which ignores the problem of the direction and the stochastic properties of the saccade (assuming it to be a straight line) and gives a prediction of the final position after looking at the onset of the saccade. The estimation of the length and duration of the saccade is the more difficult part of the problem. Some empirical observations have been made and on the basis of these, we have developed a predictive procedure--based on the velocity of the eye movement. This will be described in detail.

2. The Prediction of the Location of Eye Fixation

By using the eye-movement velocity information, we developed and

implemented a scheme for prediction of a new eye position at the termination of a saccadic movement about half way before that new position has been reached by the eye. The scheme is based on the observation of eye-movement velocity. The velocity during a saccade increases to a maximum value and then decreases back to a low value. It has been observed that the velocity curve is not symmetrical around the peak. In particular, a "trailing off" of the velocity at the end of the saccade can be clearly observed in most cases. However, it has been seen that the eye travels half the saccadic distance at the peak velocity point, thus leading to the conclusion that the areas under the saccadic velocity curve before and after the peak are equal in spite of the asymmetry in the velocity curve. Thus, by detecting the peaks in the velocity curve, the distance the eye has moved since the beginning of the saccade up to the time of this peak can be doubled to get a prediction of the eye position at the end of the saccade when the eye has arrived at a new fixation point. Therefore, when a saccade is only half completed, a prediction of the eye position at its end can be made. Because of the asymmetry, the saccade duraction cannot simply be obtained by doubling the time to the velocity peak. However, the relationship between saccade duration and length has been reported in earlier studies [1] and can be used to predict the duration.

A block diagram of the scheme is shown in Figure III.1. The X and Y eye-movement voltage outputs of the Biometrics Eye-Movement Monitor are filtered by analog 6-pole Bessel filters with cut-off frequencies ranging from 50 Hz. to 200 Hz. The outputs of these anti-aliasing filters are sampled at 1000 Hz. (1.0 ms) or 500 Hz. (2.0 ms) by the A/D conversion system of the PDP-15. This digitized eye position data may

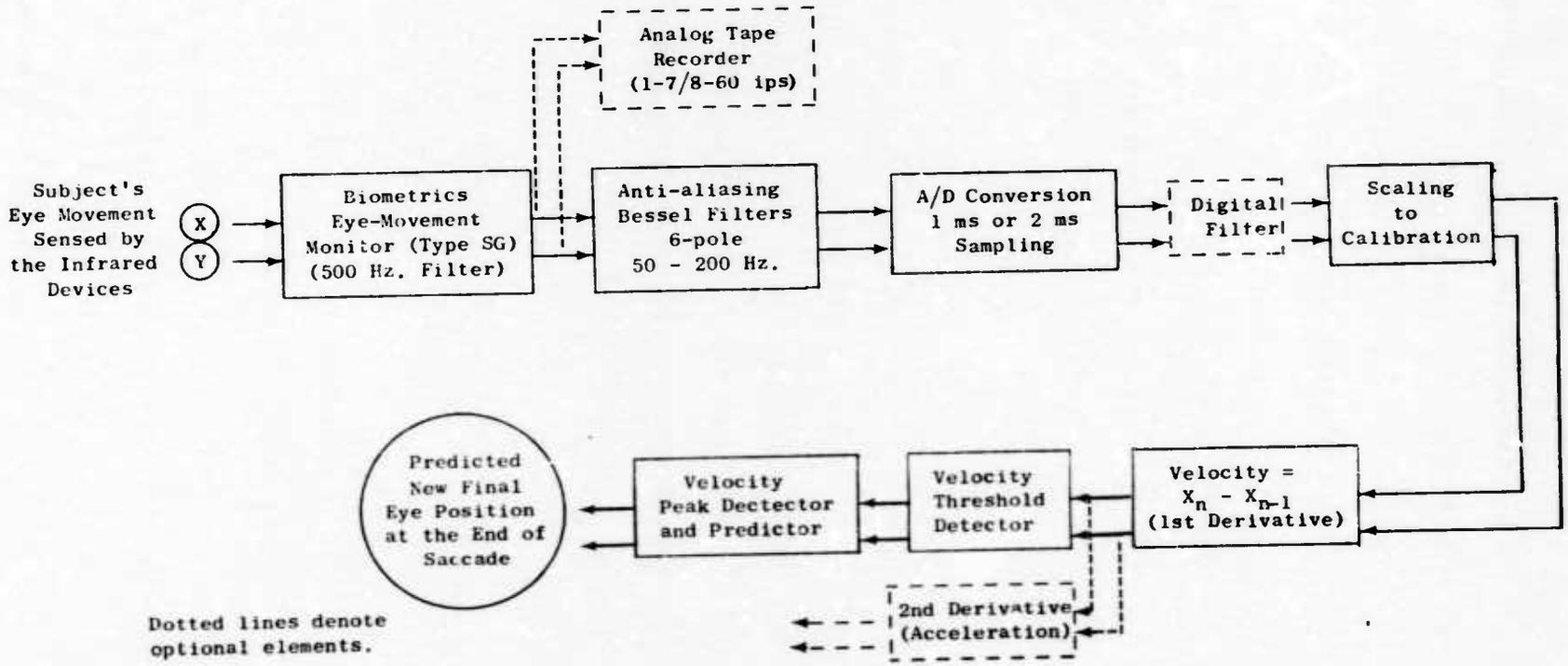

Figure III.1 Block diagram of prediction scheme using velocity information.

then be smoothed by various digital filters implemented as subroutines.

The eye-position data points are scaled according to a calibration-determined mapping function. Eye "velocity" is then calculated from these scaled position values by taking the difference between successive values:

$$\text{"velocity"} = X(n) - X(n-1)$$

where X(n), X(n-1) are two successive scaled eye-position values. This result is divided by the sampling period, T, to obtain the correct magnitude of the actual velocity.

During a fixation, this velocity fluctuates about zero with some variance, which is determined for each subject in each experiment. A threshold detector is used to monitor this fluctuation. When the velocity increases monotonically above the maximum fluctuation level, it is decided that a saccade has begun. At this time, the on-going means of the X-Y positions, which have been calculated throughout the fixations, are saved for later analysis. The peak detector now begins to look for peaks in the velocity curve. When a peak is detected, the X position value at the peak time is used in the equation below to predict what the final position will be at the end of the saccade:

$$X_{\text{final position}} = 2(X_{\text{peak}} - X_{\text{initial}}) + X_{\text{initial}}$$

$$= 2X_{\text{peak}} - X_{\text{initial}}$$

where X_{initial} is the mean value of the X position which was stored at threshold detection. The same calculations are made simultaneously to predict the Y position.

As an example, we show the prediction process in Figures III.2 through III.6. In each figure, we show the eye movement on an X-Y

plot, the horizontal (X) velocity vs. time, and the horizontal (X) eye position vs. time. In Figure III.2, we show the onset of the saccade. The intermediate eye-movement processes are shown in Figures III.3 and III.4. In Figure III.5, the velocity reaches its peak and the prediction of the fixation point is made. Finally, in Figure III.6, we show that the eyes arrive at the predicted fixation point.

Figure III.2 Onset of saccadic movement

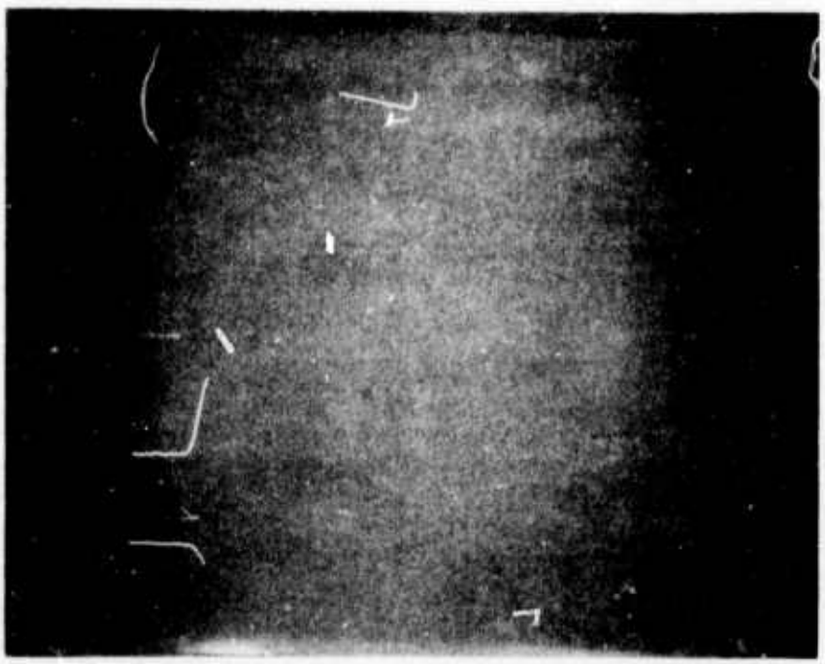

Figure III.3 Eye movement during a saccade.

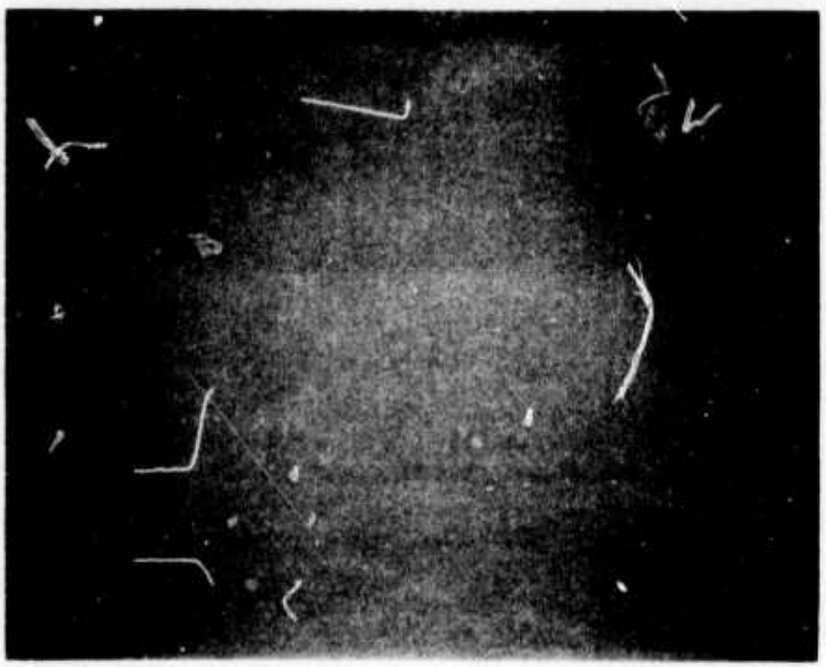

Figure III.4 Farther movement during a saccade.

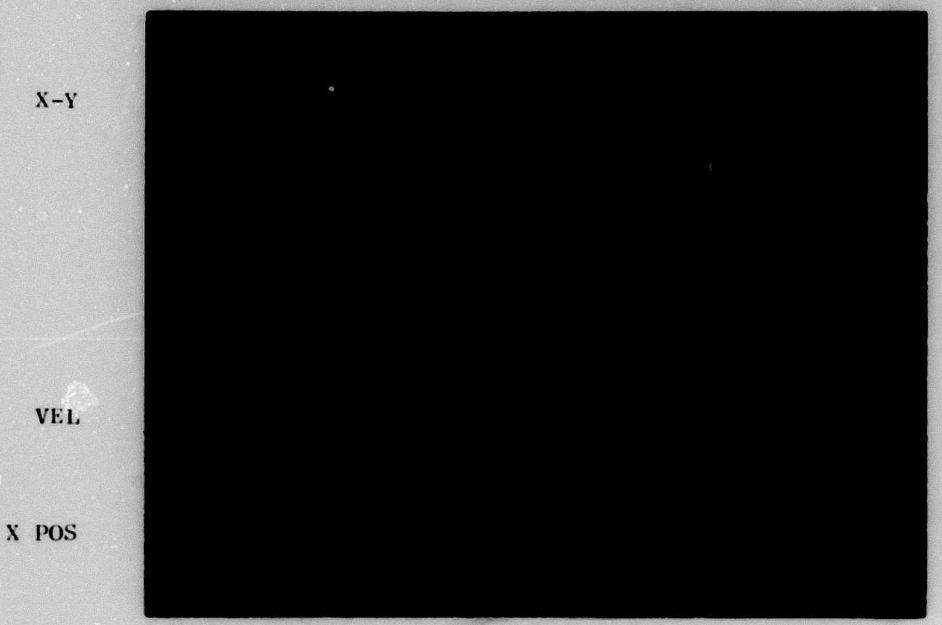

Figure III.5 The velocity of the saccade having just reached the peak value and the next fixation point predicted.

Figure III.6 The saccade terminating at the predicted fixation point.

The method just described is simple and useful; however, it restricts us to making predictions only when the eye reaches the halfway point of the saccade. It is desirable to make a prediction of final eye position at a much earlier time of the saccade. One possible means to this end is to model the saccadic process and make estimates of the parameters of the model based on information contained in the first several points of the saccade. Yarbus [1] reports that the velocity during a saccade follows a sinusoidal curve. We could fit a sinusoid to the first few points of the saccade and thus predict the peak. However, the sinusoidal function is infinitely derivable and hence susceptible to noise. We have decided to use low order polynomials instead. We are in the process of implementing this scheme. In addition, an analysis of saccades to obtain a better model is in progress.

It has been hypothesized that the eye does not observe anything during the saccadic movement. Thus, before the saccade is made, the decision is made about where to move the eye and with what velocity. Any information about these parameters in the eye-movement data should then be present in the data immediately preceeding the saccadic movement. Thus, by analyzing the fixation data just before the onset of a saccade, we can determine in what form this information is present and whether we can use it to predict the onset. Essentially, some velocity and direction analysis must be performed on this data.

For this purpose, the onset of a saccade is determined by the velocity of filtered data. When this velocity crosses a certain threshold, we mark the end of the saccade. Then a window of data, consisting of the saccade and some samples before and after the saccade (e.g., from point P_0 to P_1) are collected. For analysis, all saccades of one length

are averaged with the beginning points lined up. This smooths out the noise and generates a "typical saccade" of a given length which can be used to design a model. In another approach, the saccades are averaged with their peak velocity points lined up. From this we can determine the characteristics of the asymmetry about the peak and the relationship between the saccade length and the peak velocity.

3. Discussion

Our ultimate aim in the studying of the characteristics of saccades and fixations is to study the overall viewing of a stationary scene as a whole. It has been hypothesized that the scanpaths play an important role in the study of visual memory and we have referred earlier [2] to some theories of visual learning based on the observation of repetitive strings of fixation points during viewing of stationary, two-dimensional patterns. In the past, however, the study of scanpaths has been mostly qualitative, with determination of the existence of repetitive scanpaths being based solely on observation of the eye-movement plot by eyeballing. We have started to obtain a more quantitative procedure so that the mass of data can be reduced to a point that one can introduce some degree of objectivity in the determination and characterization of the visual scanpaths.

One approach is as follows: The field of view is divided into a rectangular N×N grid. Data are collected for many viewings of a given pattern. This is separated into fixations and saccades, each saccade being characterized by a starting cell and an ending cell. Now for each cell which is a starting cell at least once, we can get a histogram of the ending cells which will determine if there is a preferred place to which the eye travels from a certain cell. By connecting the

high occurrence saccades, we can generate a scanpath.

It was observed from this approach that many times the movement between two points is broken by intervening fixations on the same line. Hence, instead of the ending cell histograms, direction (of the saccade) histogram from each starting cell may be more useful. Work on this is in progress.

References

[1] Yarbus, A. L., Eye Movements and Vision, New York: Plenum Press, 1967, pp. 136-137.

[2] "First Annual Report on Biocybernetic Factors in Human Perception and Memory", Rpt. No. SEL-73-026, Stanford Electronics Laboratories, Stanford University, 1973.

IV. SCENE-DIFFERENCE STUDY: METHODS AND ANALYSIS

1. The Scene-difference Experiment

Sensory information processing systems in nature, and the visual system of man in particular, are extremely senstive to differences in the properties or characteristics of certain kinds of stimuli. Classical studies of stereo acuity and vernier acuity, for example, demonstrate how well two types of visual discrimination can be made. Therefore, as a goal for our research in visual memory, we decided to pursue the idea of measuring visual memory capacity through the measurement of ability to detect differences in two nearly identical scenes.

The experimental procedure, in essence, is as follows: An observer is presented with a visual scene or pattern ("the inspection figure") and is told to look at it carefully and remember as much about it as possible. Some time later, another, nearly identical, scene is presented ("the test figure") and the observer is asked whether or not the scenes are identical.

By running such an experiment we wish to gain additional insight and to collect data on some of these questions:

1. What can be said about similarities or differences in the scanpath used by different subjects or the same subject in viewing the inspection figure?
2. What similarities are there between the "inspection scanpath" and the "test scanpath"?
3. What scanpath strategy is used by different subjects in detecting differences between scenes?
4. What types of changes to the scene are easily detected by our observers, and what changes are not?

5 What differences in test scores or scanpaths may be found by subjects with eidetic imagery?

6. EEG correlates to the scanpath and detection strategies.

Thus, there are dual uses for data obtained from this study: analysis of the methods used for detecting scene differences, and analysis of repeated scans of the same visual material.

The stimulus which we selected for our intital studies is the still life scene shown in Figure IV.1. In designing an experiment such as this there is a wide range of visual stimulus material available, roughly divided into the following three categories:

a. Highly detailed scenes, rich in colors and textures.

b. Impoverished scenes, such as black and white line drawings.

c. Degraded scenes, low in contrast or containing much visual noise.

We chose our stimulus from the first category. This allows us to compare our results with many previous studies of scanpath measurements of natural scenes, and the impoverished and degraded images required for the second and third categories may be obtained from the original scene. One difficulty with using such a highly detailed scene, however, is that it becomes very difficult to quantitatively measure the magnitude of any changes made.

2. Experimental Method

A series of 35 mm slides was prepared portraying the still life as shown in Figure IV.1. One of these slides was designated the "standard" slide and the remaining slides differed from the standard in some way, usually through an addition of, deletion of or change of one component

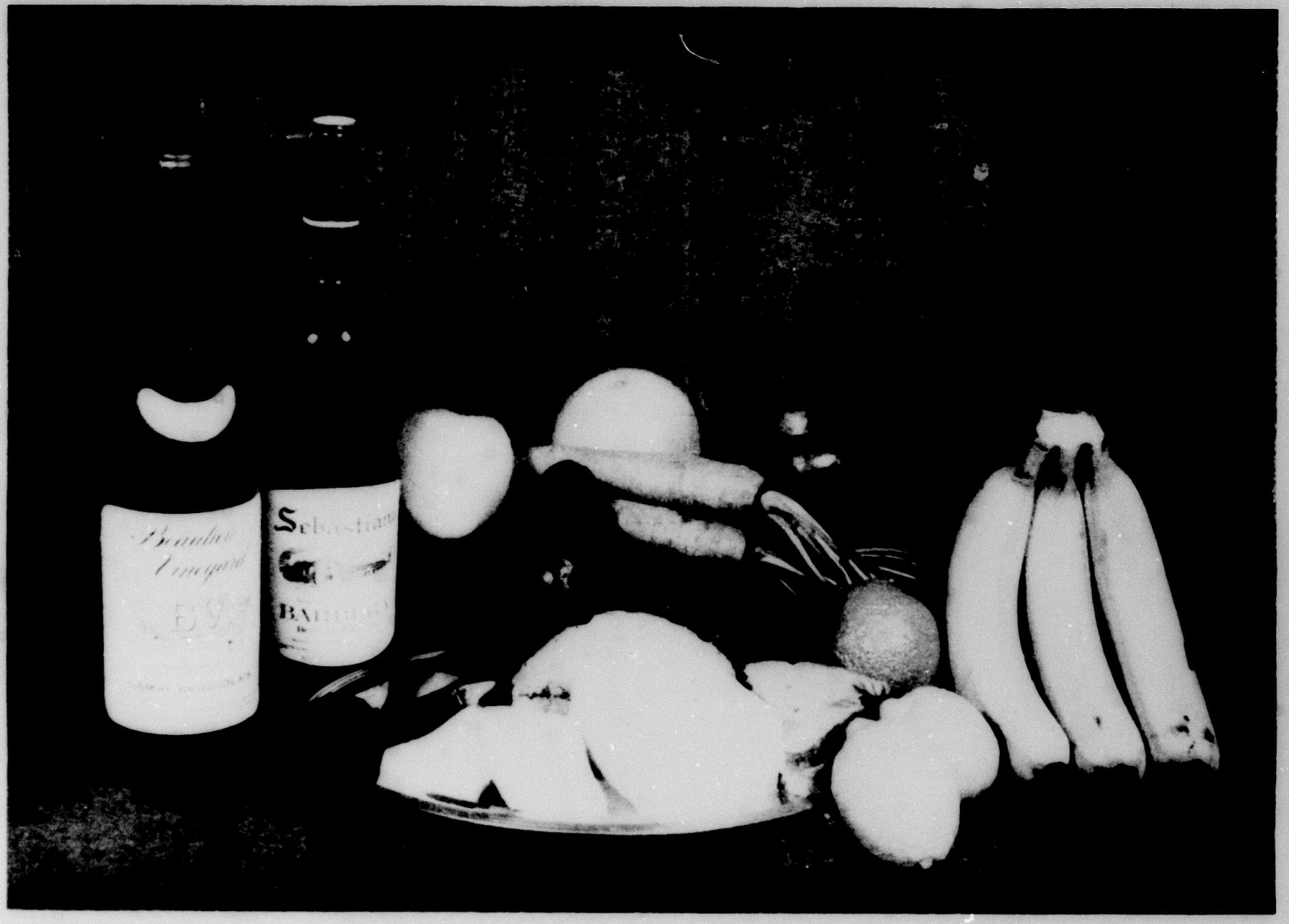

Figure IV.1 Still life "standard" scene

in the still life scene. The slides were projected on a ground glass screen located 41 cm. in front of the subject. At this distance the slide covered an angular field of 30^{o} width. Eye movements were recorded using a Biometrics SGH/V-2 monitor. The vertical and horizontal output signals were digitized using an analog-to-digital converter and then written on a digital magnetic tape. A computer analysis of the digitized data, using programs and algorithms described elsewhere in this report, converted the input data into a sequence of fixation positions and fixation start-stop times. Figure IV.2 is a record of the scanpath derived by this program superimposed on a sketch of the original scene.

The subjects were undergraduates at Stanford and each had 20/20 vision. Eye positions were calibrated using a 9-point calibration array.

An experimental session consisted of the presentation of 25 pairs of slides, the first slide of each pair being the standard slide. The standard was presented for 10 seconds, and then the test slide was presented after a delay of one second. The subject was instructed to press one of two buttons, one button corresponding to a change in the scene, and the other corresponding to no change. The slide was removed as soon as either button was pressed, and after a short delay, the standard appeared once again. The sequencing of slides and running of the experiment was under computer control.

3. Preliminary Analysis of Scanpath Differences

This experiment was run by using a number of different observers. Our initial attempt in analyzing the data is to gain insight for characterizing the scanpaths. Figures IV.3 through IV.6 are representative

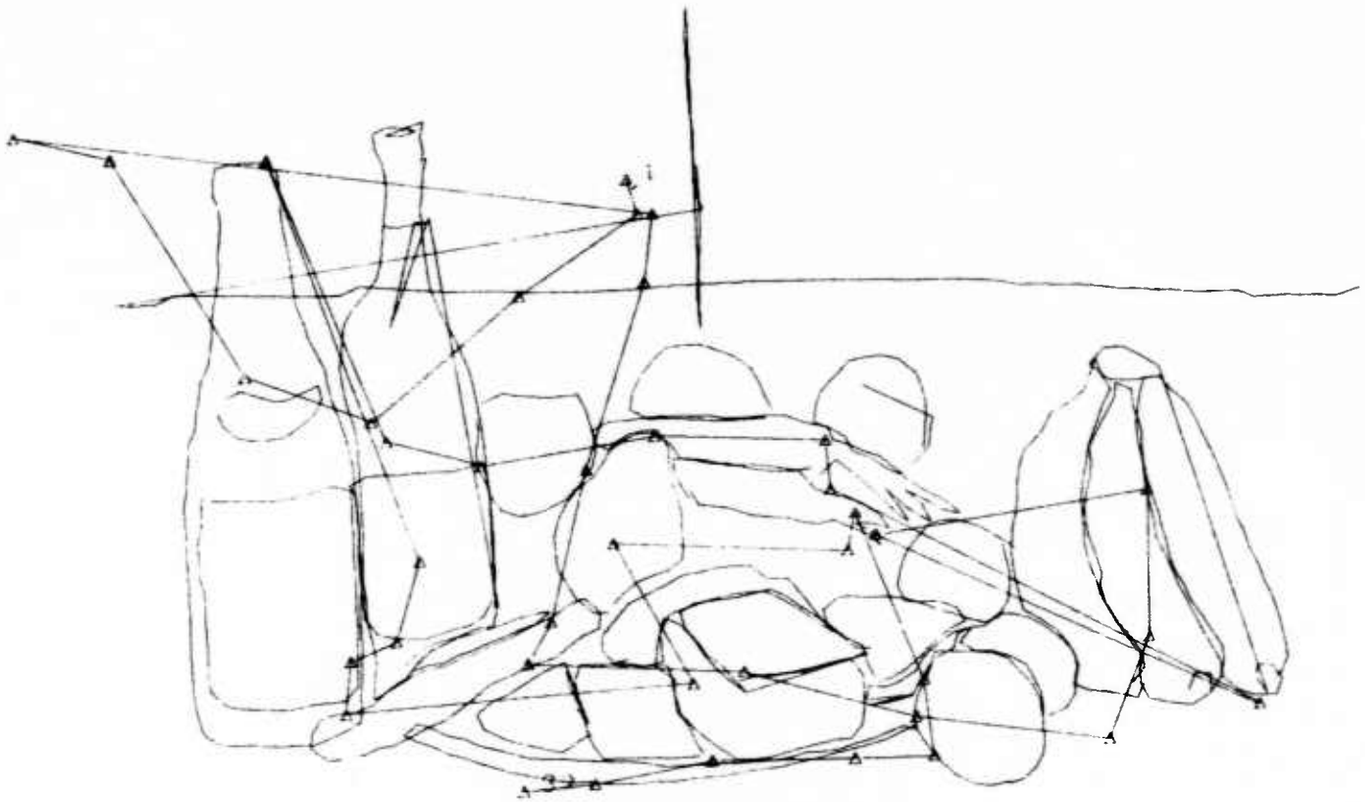

Figure IV.2 Computer derived scanpath superimposed on sketch of original scene

of the results of this preliminary analysis. Our attempt is to study all possible means for quantative characterization of the visual scanpaths. Since a scanpath is composed of a sequence of fixations and saccades, we try to scrutinize various properties of the fixations and saccades in this preliminary analysis. In Figure IV.3, we plot the number of fixations versus elapsed time. The elapsed time in seconds from the presentation of the slide is given on the horizontal axis. The total number of fixations is given on the vertical axis. The slope of the line is approximately four fixations per second, which means that the average saccade plus fixation time is 250 milliseconds. In order to ascertain some statistical properties of fixations, we made plots of fixation-duration histograms. A typical histogram is shown in Figure IV.4. Fixation times were sorted into 50 millisecond bins and the resulting histogram is plotted in the figure. Mean fixation duration time for the single scan shown is 215 milliseconds. In Figure IV.5, we present a plot of fixation duration versus fixation number. This graph illustrates the fixation time for each fixation in the scan. A systematic study of saccadic distances has been made. A typical result is shown in Figure IV.6. The distance in degrees of visual angle between sequential fixation points is plotted on this graph. A small angle approximation was used to compute the distance.

4. Foveal Fixation Plots

One benefit of computerized recording and analysis of scanpaths is that it permits transformations of the data which can lead to insights which would otherwise be lost. A graphic illustration of our ability to perform such transformations is shown in the foveal fixation plots

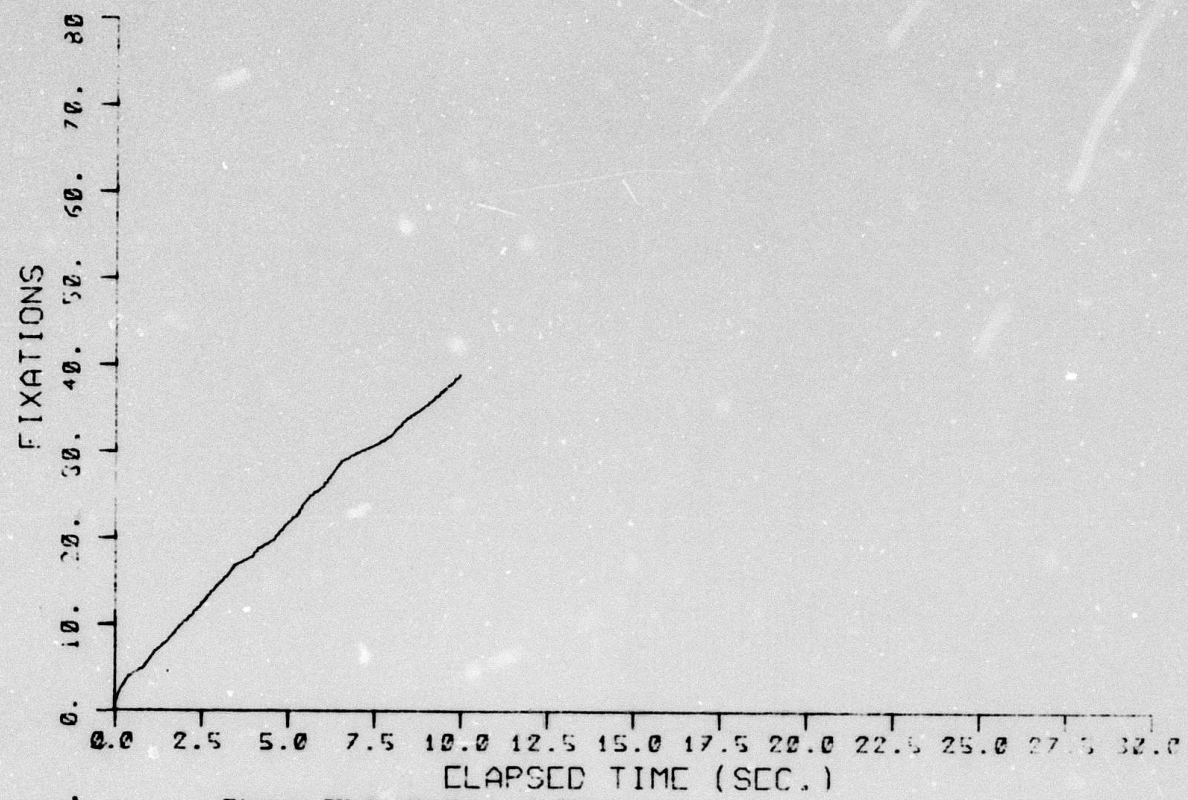

Figure IV.3 Number of fixations versus elapsed time

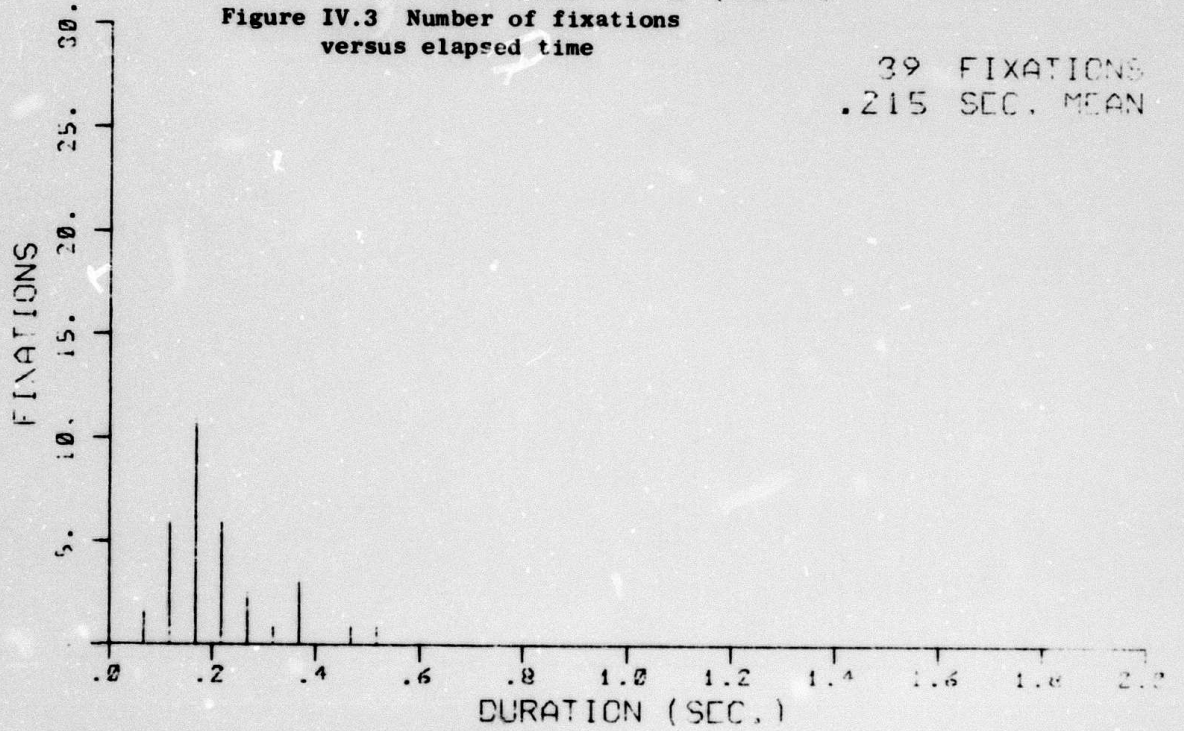

Figure IV.4 Fixation-duration histogram

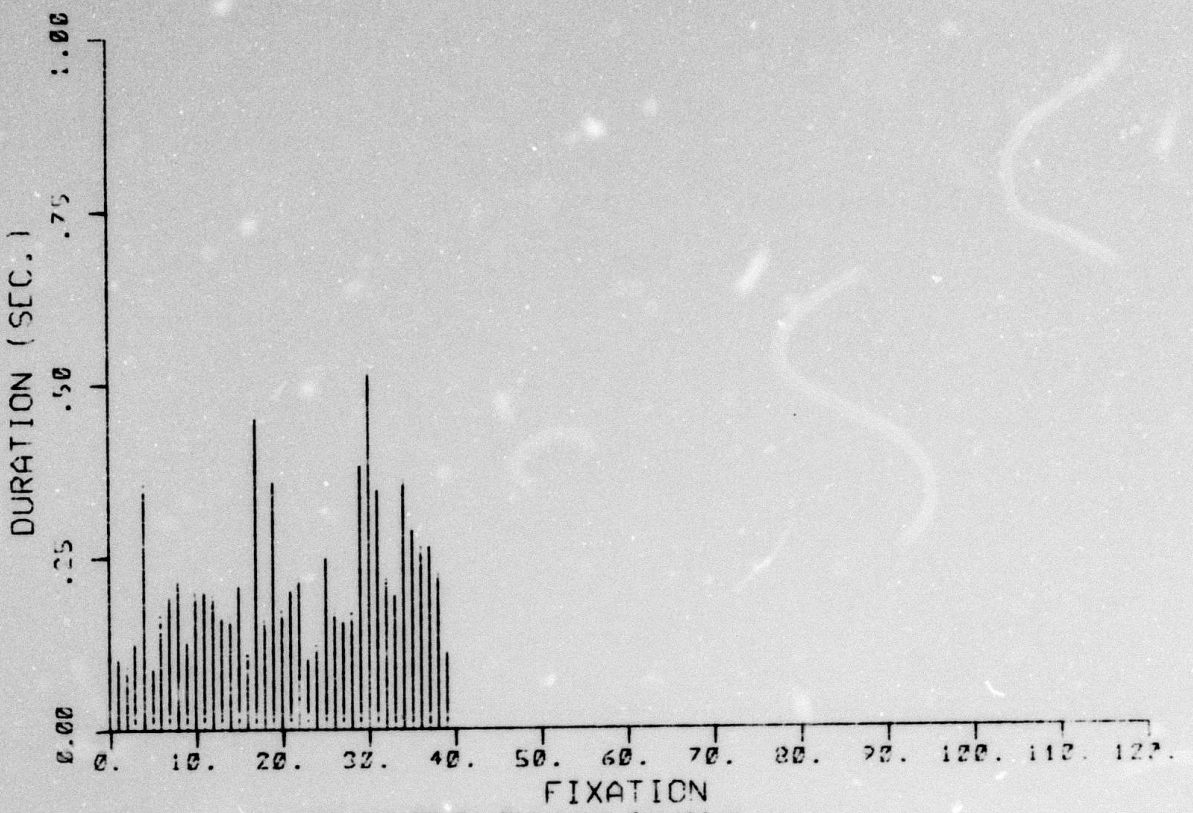

Figure IV.5 Fixation duration versus fixation number

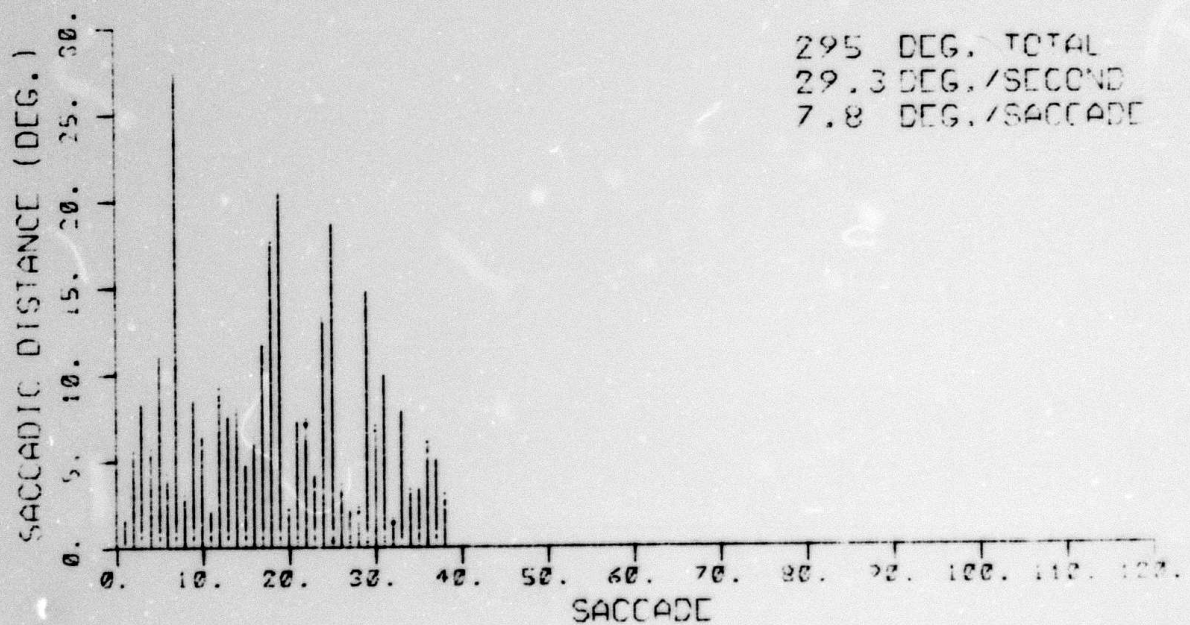

Figure IV.6 Saccadic distance versus saccade number

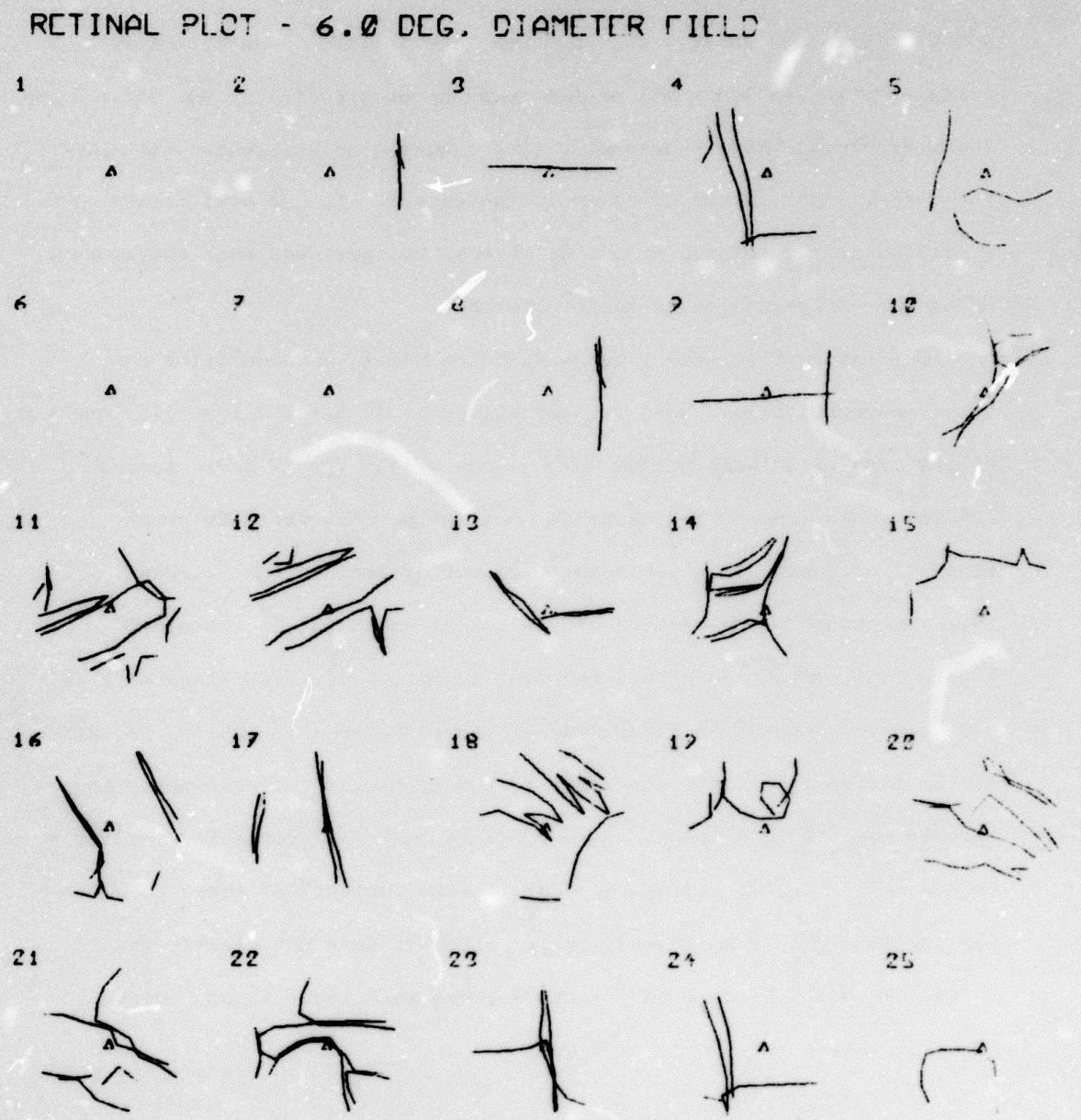

Figure IV.7 Sequence of foveal fixations

of Figure IV.7. Using the first 25 fixation points shown in Figure IV.2, we have plotted a sketch of the visual stimulus impressed on the fovea for each fixation point. The sketches show a field 6^{o} in diameter, a region which includes all of the fovea under practically any definition. These drawings, then, represent a time sequence of snapshots which are the visual input to the observer in the experiment. He must create a unified picture of the object or objects being viewed from the sequence of picture fragments shown in the sketches.

Our interest in this type of fixation point representation has three sources. First, as discussed above, it is an excellent illustration of the problem of mapping scattered pieces of the visual world into a unified whole. Next, the sketches confirm the fact that the great majority of "next" fixation points are not present in the "current" foveal region. Independent verification of this fact is contained in Figure IV.6, which shows that the mean number of degrees per saccade is 7.8, greater than twice the radius of these sketches. Finally, isolation of the foveal fixations gets right to the problem of understanding why certain regions of a visual scene are more heavily favored for fixations than others. Merely saying the "information content" of these regions is higher than that of their neighbors does not clarify the issue. We would like to be able to analyze this information content in other than a very qualitative way.

5. Scanpath Similarity Measures

In studying the scanpaths created by different observers in this experiment it is very desirable to have some measure of the similarity between two scanpaths or scanpath segments. We are currently exploring

several functions which give us an objective measure of the similarity between two fixation points and the similarity between two saccades. We have used the saccade similarity function to derive a special type of saccade density map showing the most heavily traveled routes in the visual field. We attempted to use these functions to detect cyclic or periodic sections in scanpaths. Works pertinent to this area are in progress.

V. REAL-TIME SCANPATH ANALYSIS

We have reported previously on automatic methods for the off-line analysis of scanpaths. We shall now describe a real-time method for the analysis of scanpaths. An effective real-time scanpath analyzer is an essential development in the process of implementing cybernetic models for the prediction and control of ongoing eye-pointing behavior.

This computer program has been implemented on an SEL-840 computer which has an Evans and Sutherland display system. Two large CRTs are utilized: (1) a monitor scope on which are displayed the various analyses that are of interest to the experimenter, and (2) a stimulus display CRT which is viewed by the experimental subject.

The subject is seated in front of the stimulus CRT, with head-holder and chin rest, and with the distance between the eye and the CRT surface adjusted so that 12 inches in either the vertical or horizontal dimension on the scope corresponds to 20^{o} of visual angle. (An alternative to the head-holder/chin rest is to use the Systems Technology eye point-of-regard system that essentailly monitors the subject's head position through a movable attachment to a bite-piece held in the subject's mouth. The combined inputs from the head-position monitor and the Biometrics eye-position monitor are then translated into X and Y outputs indicating the eye point-of-regard.) The subject is asked to fixate on a spot displayed on the center of the CRT. Offset voltages are adjusted in the X and Y lines so as to center the monitored eye location on the stimulus spot on the experimenter's CRT. The subject is then asked to fixate another spot located 10^{o} (or 6 inches) to the nasal side of the central fixation point. The X gain is then adjusted to make the stimulus spot and the eye-fixation monitor agree. The same procedure is followed

with stimulus spots located 6 inches above, 6 inches to the temporal side and 6 inches below the central fixation spot. Insofar as discrepancies appear between the amplifier gains suitable for the nasal 6 inches and the temporal six inches, on the one hand, or between the upper 6 inches and the lower six inches, on the other hand, the issue is resolved in favor of accuracy in the nasal sector in the case of horizontal measurements, and in favor of accuracy in the lower sector in the case of the vertical measurements. Having run through these adjustments several times, we then either choose to accept the remaining nonlinearities or we may elect to attempt differential linearization of subdivisions of the visual space.

Now, the subject is presented with a cartoon-type stimulus (out of digital storage) on his display scope and instructed to examine it freely for a specified number of seconds, after which the cartoon disappears and the central fixation spot is restored. While the subject is examining the cartoon, the X and Y voltages from the eye monitor are entered into X and Y voltage distribution tables (see Figure V.1). The entries in the tables are cumulated in accordance with a sliding time-window (the width of the window being specified in milliseconds by the experimenter). The peak of each distribution (X and Y) is treated as the best estimate of the eye pointing during the time constant characterizing the width of the sliding window. This X,Y location is made by the center of a circle (solid line) the radius of which is controllable by the experimenter. We sometimes refer to this circle as a "fixation circle" or as a "target circle" depending upon the experimental use being made of it. If we set minimum amplitude criteria for the distribution peaks, we have a basis for monitoring the "dwell time" or "spatial invariance" as a function

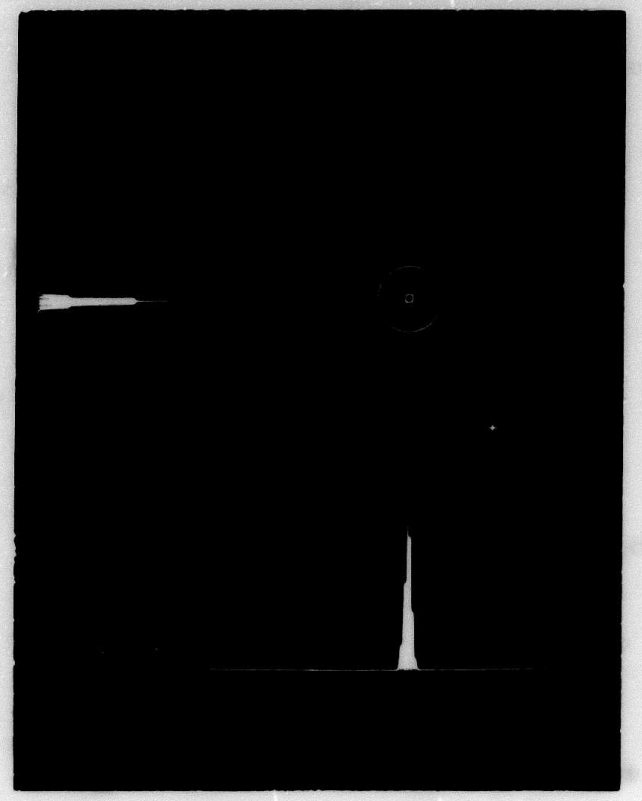

Figure V.1 Real-time eye-fixation monitor. CRT display of X and Y distributions, instantaneous eye position (small square), target circle (solid perimeter), variance circle (dotted perimeter), prior fixation (cross), and ON indicating that the square has been inside the solid circle for the required number of milliseconds.

of time, this is a reasonably effective way of defining the beginning of each fixation. The method for defining the end of a fixation is described in the next paragraph.

A second circle, sharing the same center as the target circle, has an independently variable radius which is equal to or greater than that of the target circle. This circle, which appears on the

monitor scope as a dotted line (see Figure V.1), is used to set a spatial variance limit around the target circle. When the instantaneous eye-position exceeds the perimeter of the variance circle, it is assumed that the eye is making a saccadic movement, or at least, that it is moving sufficiently far away that the information accumulated in the distributions is irrelevant, so the distributions are re-set to zero and the existing target circle vanishes.

Another important feature of this program is the arrangement whereby if the instantaneous eye position (the small square inside the target circle in Figure V.1) remains inside the target circle for a specified number of milliseconds (determined by the experimenter), a voltage appears on an appropriate analog output line and the word ON is displayed on the monitor scope until the instantaneous eye position travels outside the target circle; then the output voltage goes to ground the the word OFF replaces the word ON (see Figure V.2).

This program provides for the storage of 100 fixation locations or 100 specified target centers. In the analysis of a scanpath, a cross appears at each fixation location and each cross is numbered in accordance with the ordinal position of the fixation in the scanpath.

We are also studying whether guiding the subject to his earlier scanpath fixation locations has a favorable effect upon image recognition. We are entertaining the hypothesis that one feature of superior concrete memory is an unusual consistency in retracing scanpaths. In other words, a possible difference between good concrete memory and poor concrete memory is that the former remembers not only what was seen but also where it was seen, whereas the latter may remember what but not where. If this were true, guiding the later to the appropriate location should

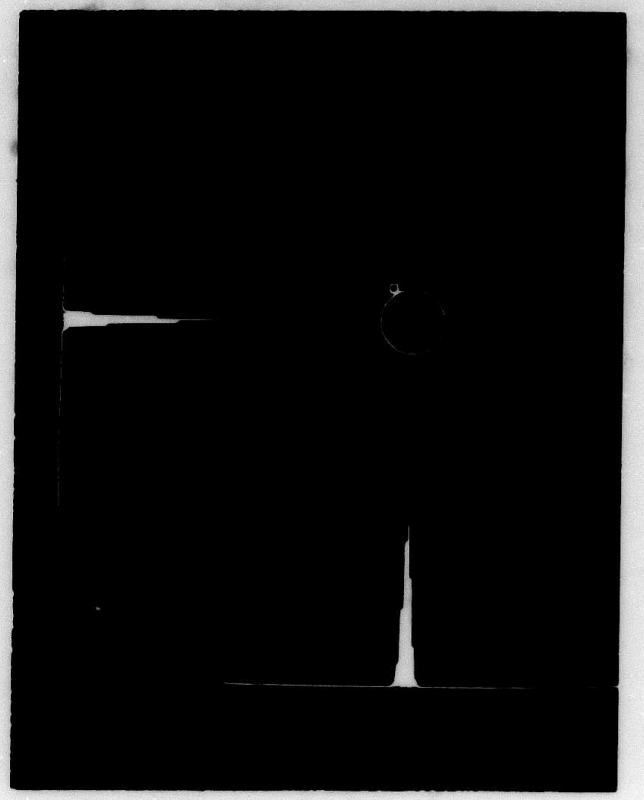

Figure V.2 Real-time fixation monitor.

Similar to Figure V.1 except that the instantaneous eye position is outside the target circle. OFF means "off target" and indicates that the associated analog output voltage is at ground.

enhance recognition of the contents of scenes previously examined (scanned).

VI. MODELING OF EEG SIGNALS DURING PHOTIC STIMULATION

1. Introduction

To better understand the relation between visual stimuli and the EEG signal, we have used a nonlinear oscillator to model the stimulus-response relationship. In particular, we are studying the entrainment of the alpha rhythm by periodic photic stimuli. This will enhance our understanding of the effect on EEG signals exerted by the repetitive photic stimulation and the various degrees of efficiency of the stimulus falling on various phases of the EEG signal. There is every reason to believe, based on the results of other researchers, that the eye takes in information only when it is fixating. One of our goals is to guide the eye to fixate only at those instances corresponding to the EEG phases while the brain is in the best state for processing information. We believe that there are relations between the effective phases for stimulation and the optimal phases for fixations. It is hoped that the development of a model for the entrainment process will elucidate the the behavior of the alpha frequency and phase, and thus lead to a more practical brain state estimator and predictor for use in our memory studies.

During the past year, significant progress was made toward establishing such a model for a class of EEG phenomena. The work began with a search for an alertness estimator for use in interpreting EEG data taken during eye-movement studies, since one of the major factors influencing the data collected is drowsiness or level of alertness of the subject. It was thought that the degree of alpha rhythm entrainment by periodic photic stimuli might be a good alertness index. A nonlinear model of the entrainment phenomenon was developed, and has

subsequently predicted a number of unexpected related phenomena. We will discuss the model, the EEG data, and simulations of the model.

2. A Mathematical Model for Photic Entrainment of EEG Signals

We will show that the entrainment behavior of the alpha rhythm can be modeled by a type of nonlinear oscillator first studied by Van der Pol. The model is concerned primarily with the nonrandom periodic component of the EEG, although it is hoped that some light will be shed on transitionary behavior, such as visual evoked responses.

We denote the EEG signal by $u(t)$ which is assumed to satisfy the nonlinear differential equation below during periodic stimulation:

$$\ddot{u} - \epsilon(1 - u^2)\dot{u} + \omega^2 u = B \cos \nu t + B_0 \qquad (1)$$

where ω is the unstimulated alpha frequency, ν is the stimulus frequency, B is the stimulus amplitude, B_0 is the stimulus bias level, and ϵ controls the amount of nonlinearity in the system. It is proposed that ϵ is related to a certain psychophysiologic state and mathematically represents the amount of coupling between the brain and its environment. This equation assumes a sinusoidal stimulus (typically $B_0 = B$) since the analysis is simple. Our experiments to date have used a pulsed stimulus, and the resulting differences will be discussed in the section on simulation.

Letting $x = \omega^2 u - B_0$ in (1), we get

$$\ddot{x} - \frac{\epsilon}{\omega^4}\left(\omega^4 - B_0^2\right)\left[1 - \frac{x^2 + 2xB_0}{\omega^4 - B_0^2}\right]\frac{\dot{x}}{\omega^2} + x = B \cos \nu t$$

or

$$\ddot{x} - \mu(1 - \beta x - \gamma x^2)\dot{x} + \omega^2 x = \omega^2 B \cos \nu t \qquad (2)$$

where $\mu = \frac{\epsilon}{\omega^4}\left(\omega^4 - B_0^2\right)$, $\beta = \frac{2B_0}{\omega^4 - B_0^2}$, $\gamma = \frac{1}{\omega^4 - B_0^2}$.

For simple entrainment, where $\nu \approx \omega$, we expect a solution of the form

$$x_0(t) = b_1 \sin \nu t + b_2 \cos \nu t \quad . \tag{3}$$

Substituting (3) into (2):

$$\begin{aligned}
&-b_1\nu^2 \sin \nu t - b_2\nu^2 \cos \nu t \\
&-\mu(1 - \beta b_1 \sin \nu t - \beta b_2 \cos \nu t \\
&\qquad -\gamma b_1^2 \sin^2 \nu t - 2\gamma b_1 b_2 \sin \nu t \cos \nu t - \gamma b_2^2 \cos^2 \nu t) \times \\
&\qquad (b_1\nu \cos \nu t - b_2\nu \sin \nu t) \\
&+ \omega^2 b_1 \sin \nu t + \omega^2 b_2 \cos \nu t - \omega^2 B \cos \nu t = 0 \quad .
\end{aligned}$$

With a little trigonometry, we can write this in a form useful for harmonic balancing:

$$\begin{aligned}
&\sin \nu t \left[-b_1\nu^2 + \mu b_2\nu - \frac{3}{4}\mu\gamma b_1^2 b_2\nu - \frac{1}{4}\mu\gamma b_2^3\nu + \frac{1}{2}\mu\gamma b_1^2 b_2\nu + \omega^2 b_1\right] \\
&+ \sin 2\nu t \left[\frac{1}{2}\mu\beta b_1^2\nu - \frac{1}{2}\mu\beta b_2^2\nu\right] \\
&+ \sin 3\nu t \left[\frac{1}{4}\mu\gamma b_1^2 b_2\nu - \frac{1}{4}\mu\gamma b_2^3\nu + \frac{1}{2}\mu\gamma b_1^2 b_2\nu\right] \\
&+ \cos \nu t \left[-b_2\nu^2 - \mu b_1\nu + \frac{3}{4}\mu\gamma b_2^2 b_1\nu + \frac{1}{4}\mu\gamma b_1^3\nu - \frac{1}{2}\mu\gamma b_2^2 b_1\nu + \right. \\
&\qquad \left. \omega^2 b_2 - \omega^2 B\right] \\
&+ \cos 2\nu t \left[\frac{1}{2}\mu\beta b_1 b_2\nu + \frac{1}{2}\mu\beta b_2 b_1\nu\right] \\
&+ \cos 3\nu t \left[\frac{1}{4}\mu\gamma b_2^2 b_1\nu - \frac{1}{4}\mu\gamma b_1^3\nu + \frac{1}{2}\mu\gamma b_2^2 b_1\nu\right] \\
&+ \left[-\frac{1}{2}\mu\beta b_1 b_2\nu + \frac{1}{2}\mu\beta b_1 b_2\nu\right] = 0 \quad .
\end{aligned}$$

As a first approximation, we force the $\sin \nu t$ and $\cos \nu t$ terms to zero (harmonic balancing):

$$\begin{cases} b_1(\omega^2 - \nu^2) + \mu b_2 \nu - \frac{1}{4}\mu\gamma b_1^2 b_2 \nu - \frac{1}{4}\mu\gamma b_2^3 \nu = 0 \\ b_2(\omega^2 - \nu^2) - \mu b_1 \nu + \frac{1}{4}\mu\gamma b_2^2 b_1 \nu + \frac{1}{4}\mu\gamma b_1^3 \nu = \omega^2 B \end{cases}$$

or

$$\begin{cases} b_1(\omega^2 - \nu^2) + b_2\mu\nu - \frac{1}{4}\mu\gamma\nu b_2(b_1^2 + b_2^2) = 0 \\ b_2(\omega^2 - \nu^2) - b_1\mu\nu + \frac{1}{4}\mu\gamma\nu b_1(b_1^2 + b_2^2) = \omega^2 B \end{cases} .$$

Letting

$$\sigma_1 = \frac{\omega^2 - \nu^2}{\mu\nu} , \qquad a_0 = \frac{2}{\sqrt{\gamma}}$$

$$x_1 = \frac{b_1}{a_0} , \quad y_1 = \frac{b_2}{a_0} , \quad r_1^2 = x_1^2 + y_1^2 ,$$

we have

$$\begin{cases} \sigma_1 x_1 + (1 - r_1^2) y_1 = 0 \\ -\sigma_1 y_1 + (1 - r_1^2) x_1 + \frac{\omega^2 B}{\mu\nu a_0} = 0 \end{cases} \tag{4}$$

Eliminating x_1, y_1, we get

$$\left[(1 - r_1^2)^2 + \sigma_1^2\right] r_1^2 = \left(\frac{\omega^2 B}{\mu\nu a_0}\right)^2 . \tag{5}$$

Equation (5) generates the response curves for the harmonic oscillations which are plots of the amplitude r_1 as a function of the detuning σ_1 for various values of the stimulus parameter B. When $B = 0$, we have $r_1 = 1$, $\sigma_1 = 0$, and $b_1^2 + b_2^2 = a_0^2$, hence a_0 is the amplitude of the autonomous oscillation in (3).

There are two solutions when the detuning $\sigma_1 = 0$; we have seen the trivial case above, and the other case occurs when $y_1 = 0$.

When this happens, x_1 is the solution to

$$x_1^3 - x_1 - \frac{\omega_B^2}{\mu\omega_0} = 0 \quad ; \qquad b_1 = a_0 x_1 \quad .$$

Here the oscillation is $x_0 = b_1 \sin \nu t$; hence, there is a 90^o phase difference between the stimulus and EEG signals during driving at the alpha frequency. As we shall see later, this has been borne out by the analysis of real data.

For the case of subharmonic and superharmonic entrainment, the solution is of the form $x_0 = b_0 \cos \omega t + b_1 \sin n\nu t + b_2 \cos n\nu t$, where n is 1/2, 1/3, ..., or 2, 3, ..., respectively. The analysis is quite similar to the one above.

We shall next describe our simulation of this model and the resultant phenomena it produces. The simulated model predicts and accounts for many of the phenomena exhibited by real data presented in the last section.

3. Simulation of EEG & Photic Driving

The simulation is a digital computer implementation of the Van der Pol oscillator described above. A fourth order Runge-Kutta formula is used to solve the differential equation, and an FFT is used to compute the spectrum of the solution. In the figures to follow, the upper plot shows the simulated EEG signal at the time the stimulus was initiated, plus the stimulus waveform itself. The lower plot contains the power spectra of the EEG and stimulus waveforms. All simulations were done with identical parameter settings.

The stimulus used in the simulations is a pulse train since our experimental stimulus has been a stroboscope. The effect of the pulsed

stimulus is akin to that from a set of sinusoidal stimuli placed at integer harmonics. Note that superposition does not apply here.

Figure VI.1 shows the autonomous oscillation and its spectrum. The stimulus is totally absent here; the amplitude of the oscillation is fixed by the limit cycle phenomenon. This situation obviously corresponds to the closed-eye alert brain state. Figure VI.2 illustrates entrainment to a 9.0 Hz. stimulus; the alpha frequency is 9.7 Hz. Note the small response at the alpha frequency. In addition, there is a very small response at 18.0 Hz., but apparently the simulation parameters do not match the subject perfectly since its amplitude should be larger (see Figure VI.7). Parameter matching is difficult since the alertness of the subject varies widely and has a strong influence on the resulting spectrum. Figure VI.3 is a combined frequency oscillation which correctly predicts a phenomenon not previously reported in EEG literature (see Figure VI.8). Again, the second harmonic amplitude is somewhat low. Figure VI.4 predicts Figure VI.9 remarkably well; this is another combined frequency oscillation. In Figure VI.5, we see a superharmonic entrainment (some of this is due to the pulsed stimulus). Note the responses at 4.5, 9.0, 13.5, and 9.7 Hz., and compare with Figure VI.10. The simulation of subharmonic entrainments is in progress.

4. EEG During Photic Driving

The EEG potentials are measured between the occipital region and the yoked left and right earlobes with the ground electrode over the mastoid process. Left and right occipital potentials are recorded on analog tape in addition to the analysis procedures to be described. The subject is stimulated through closed eyelids with a stroboscope for 30 seconds on, then 30 seconds off. The frequency is varied between

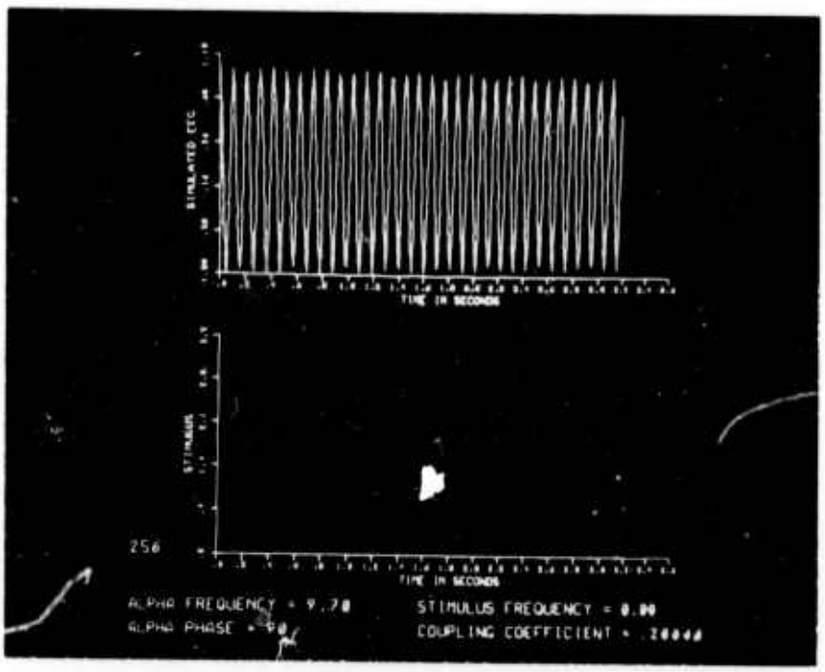

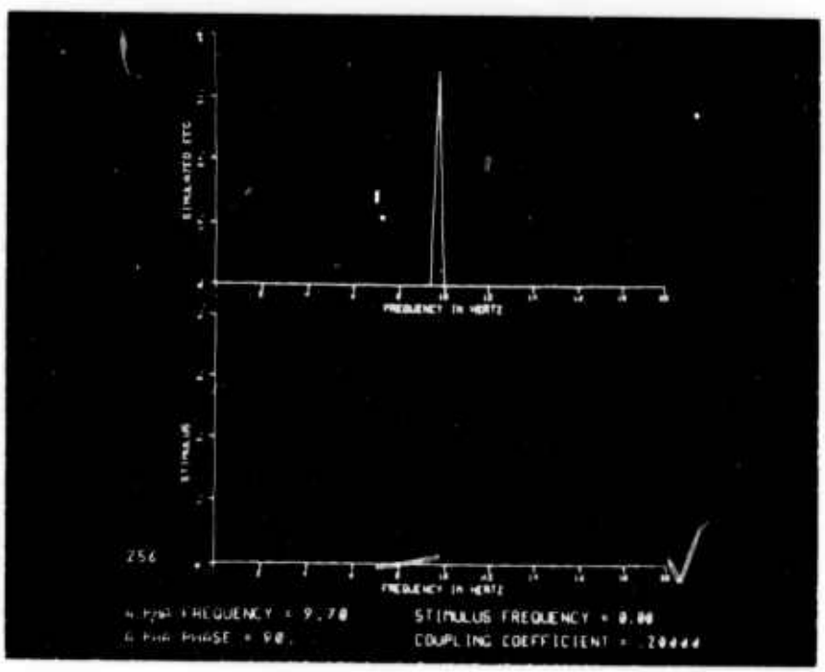

Figure VI.1 Simulated EEG in the absence of stimuli

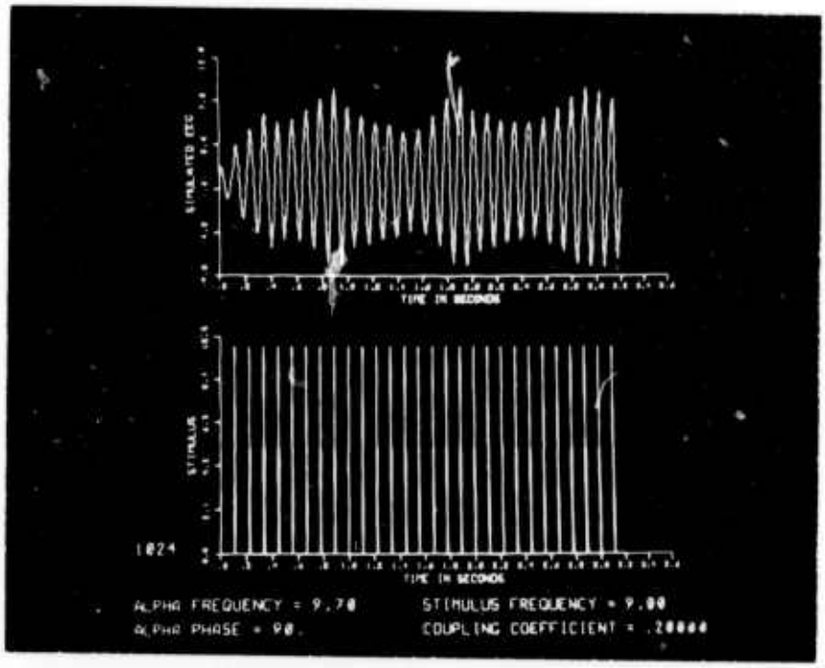

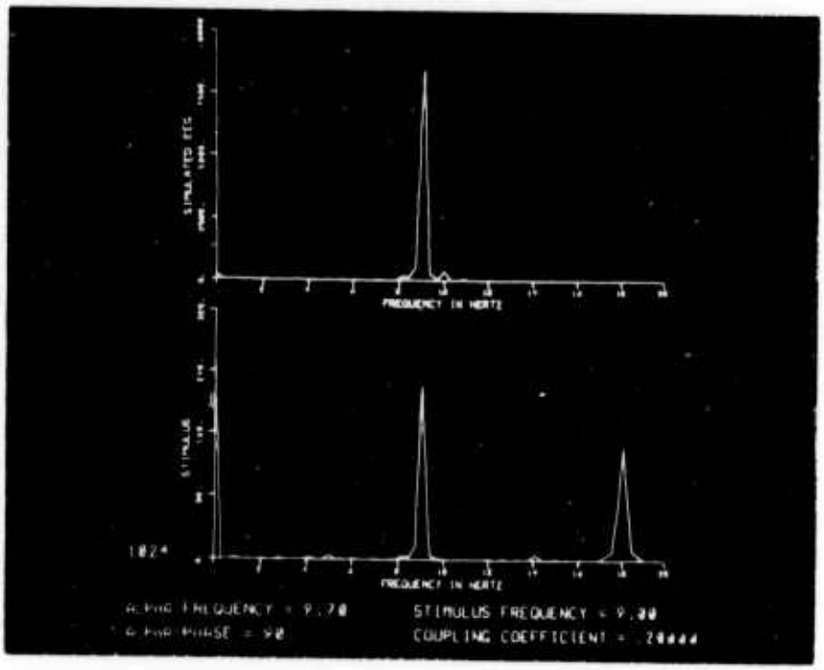

Figure VI.2 Simulated EEG driven by 9.0 Hz. Stimulus

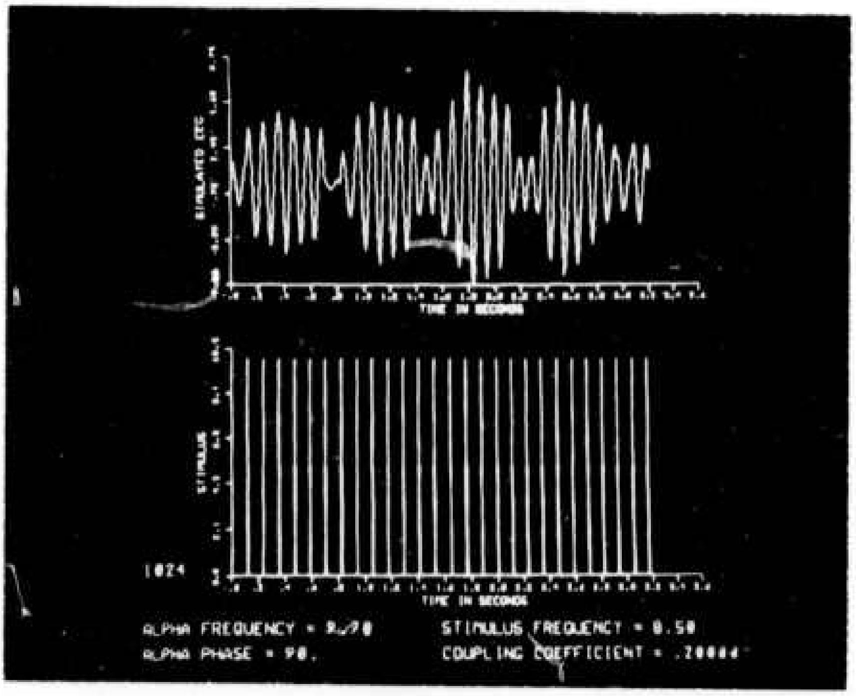

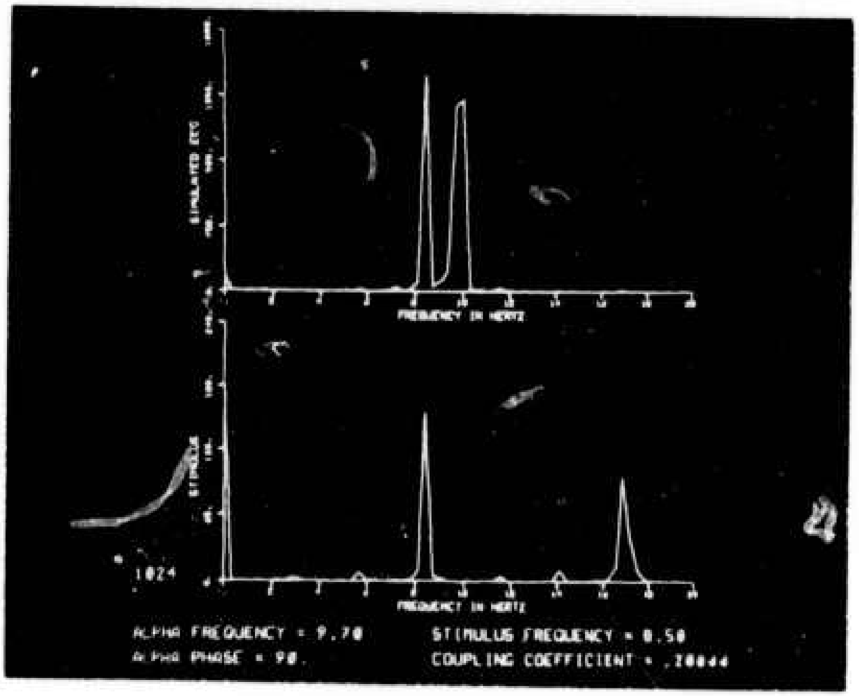

Figure VI.[illegible] Simulated EEG driven by 8.5 Hz. stimulus

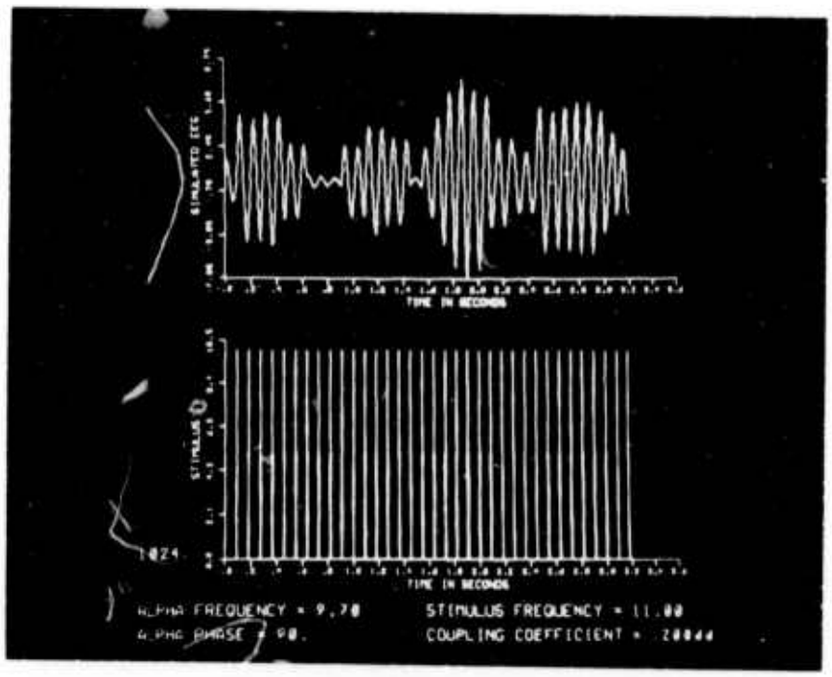

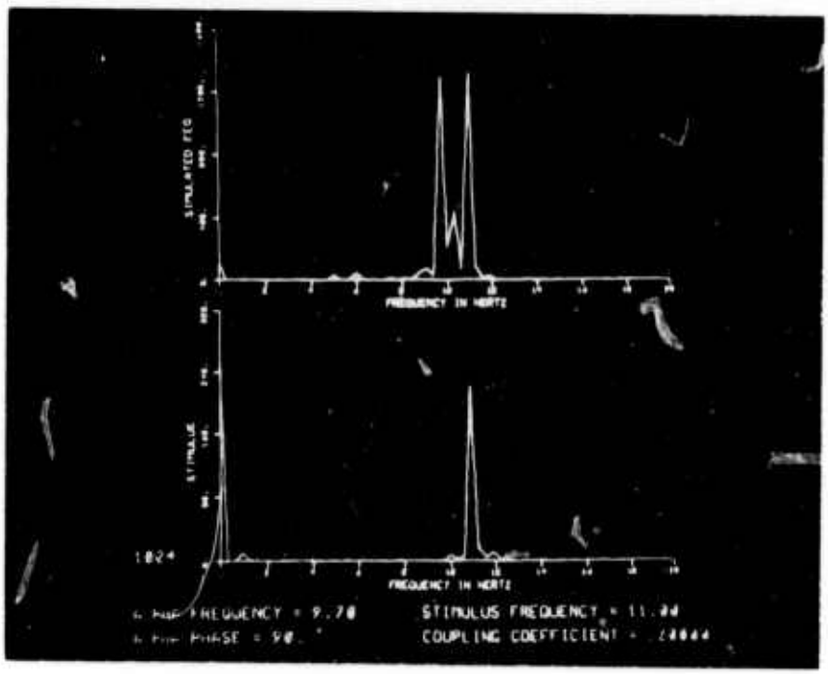

Figure VI.1 Stimulated EEG driven by 11.0 Hz. stimulus

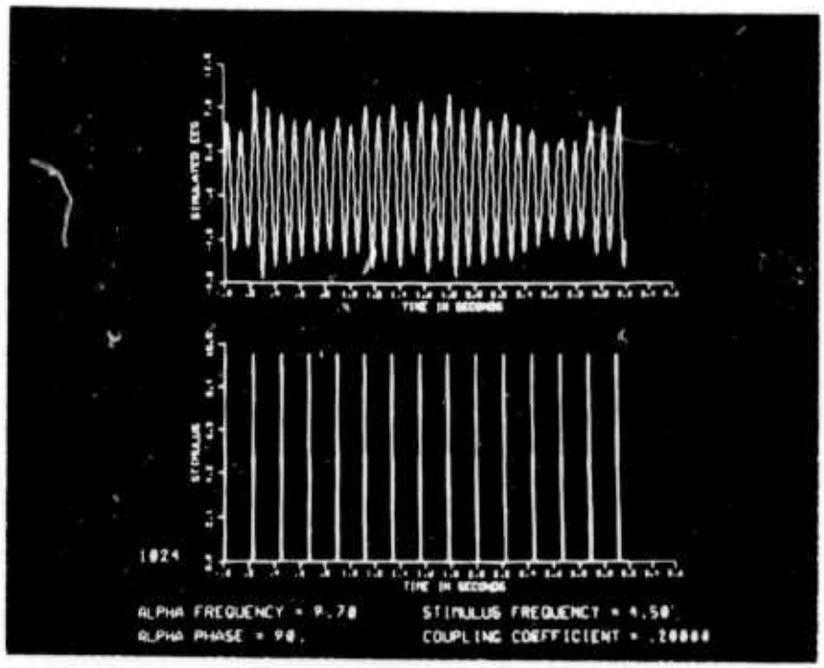

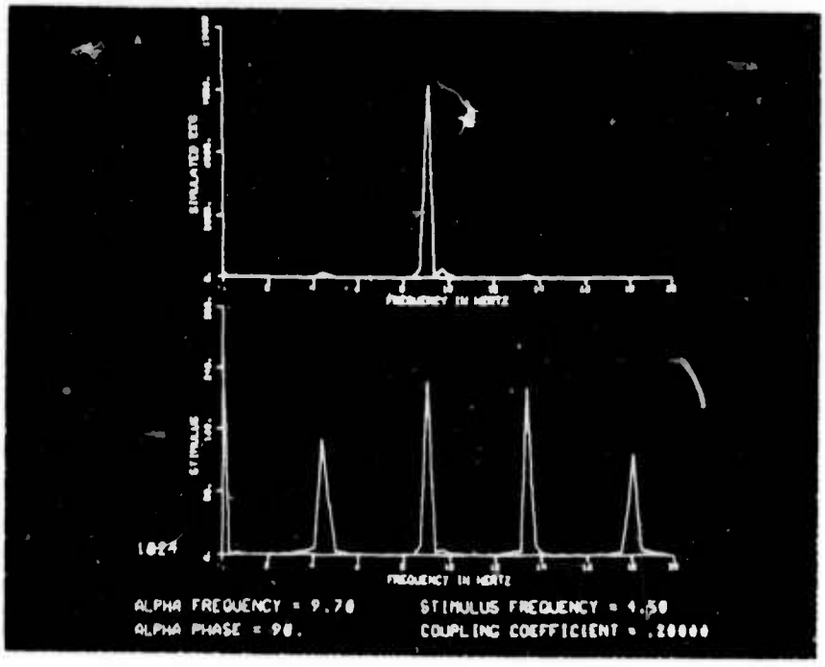

Figure VI.3: Simulated EEG driven by 4.5 Hz. stimulus

.5 and 20 Hz. in several patterns. In addition, the subject is requested to press a key once every five seconds. The variance of the inter-key-press time provide a primitive alterness index.

The EEG data is lowpass filtered with a cut-off frequency of 30 Hz., and its power spectrum is computed by a SAICOR digital spectrum analyzer and written on 9-track magnetic tape by a PDP-8. The spectra shown below are cumulative over the stimulus-on period.

Figure VI.6 is a 60-second cumulative spectral of the subject's unstimulated alert EEG. The alpha frequency here is estimated at 9.7 Hz. In Figure VI.7 we see the result of a stroboscopic stimulus at 9.0 Hz. Note that the alpha rhythm has entrained to 9.0 Hz., and that a harmonic at 18.0 Hz. also appears. In Figure VI.8 about half the power lies at the alpha frequency, and the rest is at the stimulus frequency of 8.5 Hz. and its second harmonic of 17.0 Hz. We can say that the edge of entrainment here is about 9 Hz., and that we are now seeing a combined frequency oscillation where the stimulus is at 11.0 Hz. Figure VI.10 shows a superharmonic entrainment to a stimulus of 4.5 Hz. Much of this effect is due to the integer harmonics of the pulsed stimulus, as discussed in the simulation section. Note the small response at 4.5 and 13.5 Hz. In Figure VI.11, we see a subharmonic entrainment due to stimulation at 18.0 Hz. Note the small combined frequency effect.

The spectral data is well predicted by the nonlinear model; harmonic entrainment, combined frequency responses, superharmonic entrainment, and subharmonic harmonic entrainment are all accounted for. We now turn to the 90^{o} phase prediction.

For phase calculations the EEG data is bandpass filtered with a bandwidth of 5 Hz. and a center frequency at the subject's mean alpha

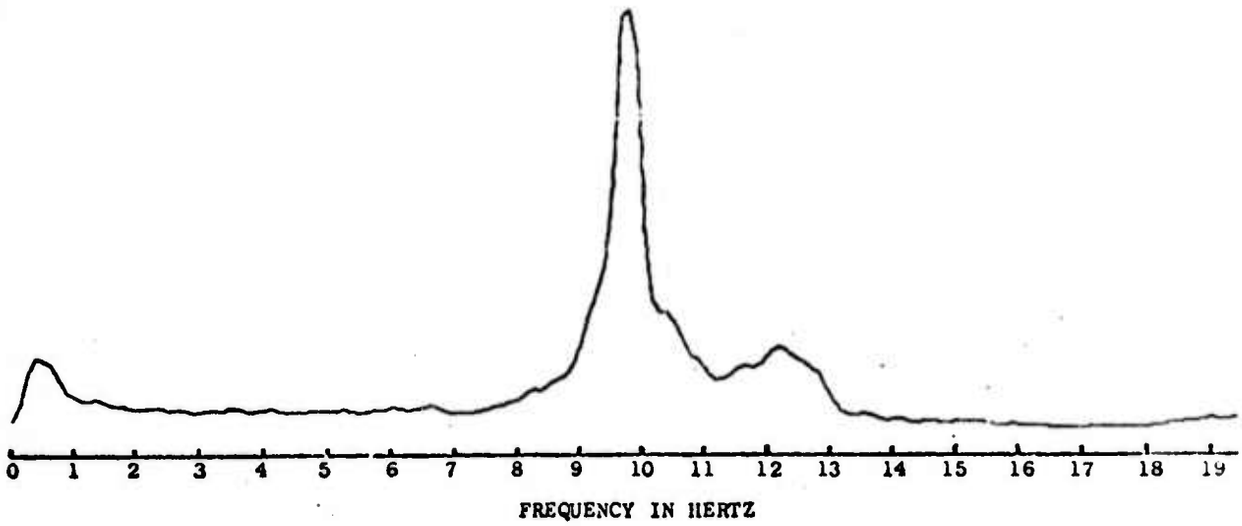

Figure VI.6 EEG spectrum in the absence of stimuli.

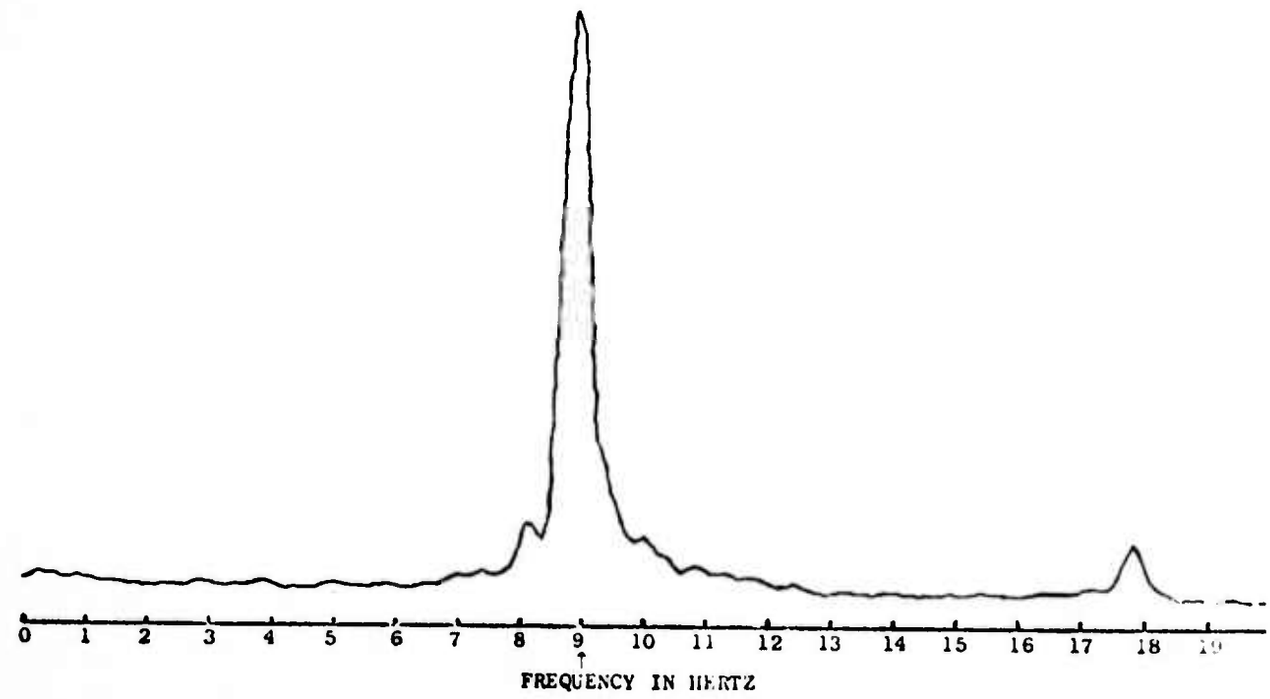

Figure VI.7 EEG spectrum during 9.0 Hz. driving

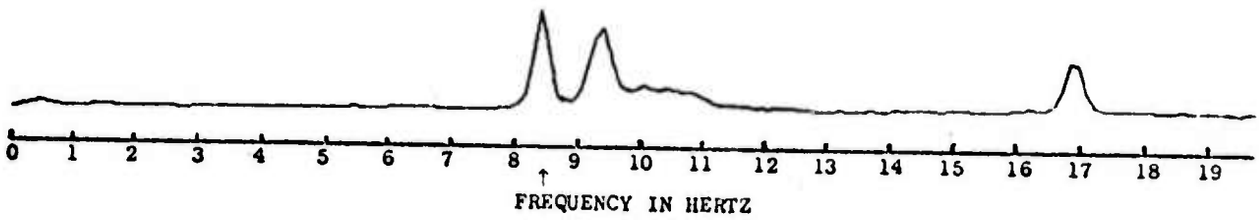

Figure VI.8 EEG spectrum during 8.5 Hz. driving.

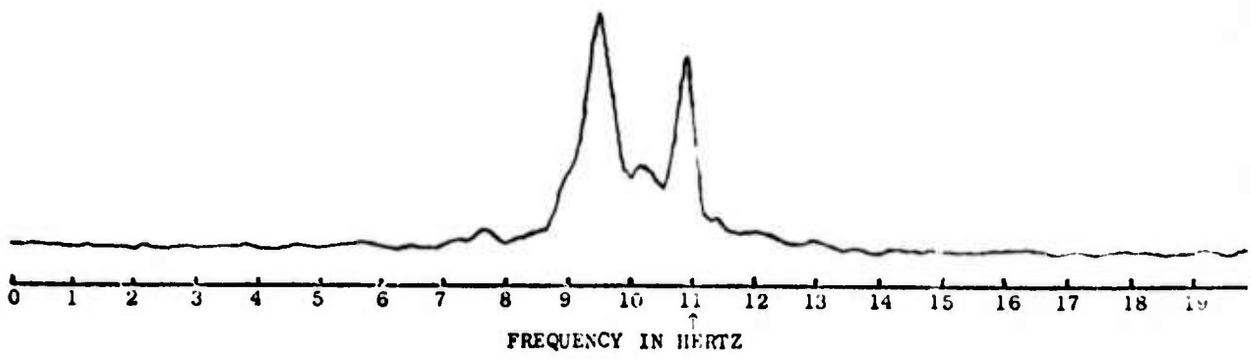

Figure VI.9 EEG spectrum during 11.0 Hz. driving.

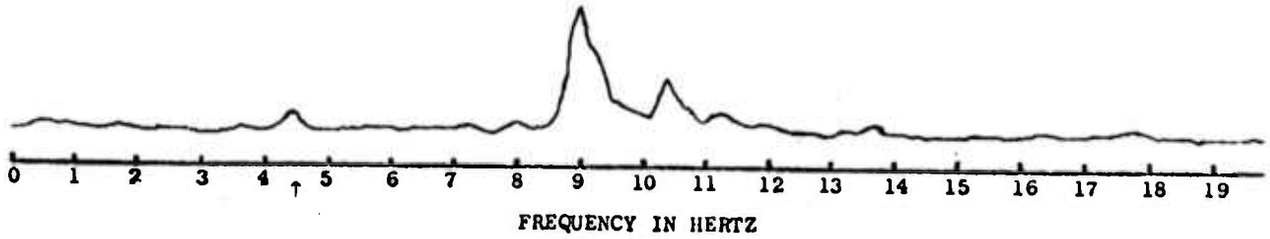

Figure VI.10 EEG spectrum during 4.5 Hz. driving.

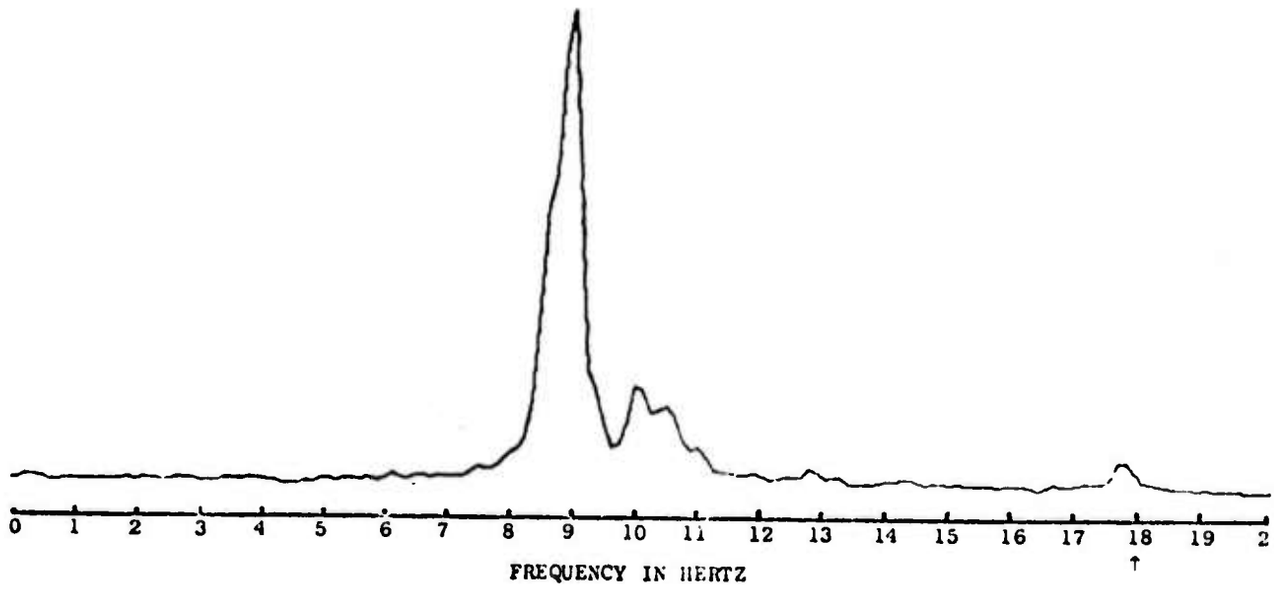

Figure VI.11 EEG spectrum during 18.0 Hz. driving.

frequency. The parameters of interest are computed online and stored digitally on magnetic tape in addition to being output on a strip chart recorded with the EEG.

The mean alpha period is determined from the period of its autocorrelation function, which is obtained once every 160 milliseconds from a digital correlation analyzer. The internal integration step is exponentially weighted with a time constant of 4 seconds to provide a reasonably stationary period. The phase between the alpha rhythm and the periodic stimulus is obtained by cross correlation, again with a time constant of 4 seconds. The hardware correlational analyses provides a simple real-time evaluation of two key parameters and minimize the computation performed by the computer running the experiment.

We show some results of this analysis in Figure VI.12. Note the changes in the alpha period and phase lag as a function of the stimulus being on or off. When the stimulus is on, the alpha period becomes 100 milliseconds, the period of the stroboscopic stimulus. When the stimulus is off, the period becomes 88 milliseconds, the autonomous alpha period of the subject. In addition the phase between the stimulus and the alpha rhythm assumes a fairly stationary value of 90 degrees when the stimulus is on and drifts at no particular value when the stimulus is off.

These experimental data clearly exhibit three of the major characteristics as predicted by the nonlinear oscillator model: the autonomous alpha frequency ω is entrained to the stimulus frequency ν; the phase lag assumes a preferred value of 90 degrees; and the autonomous rhythm ω returns when the stimulus is removed.

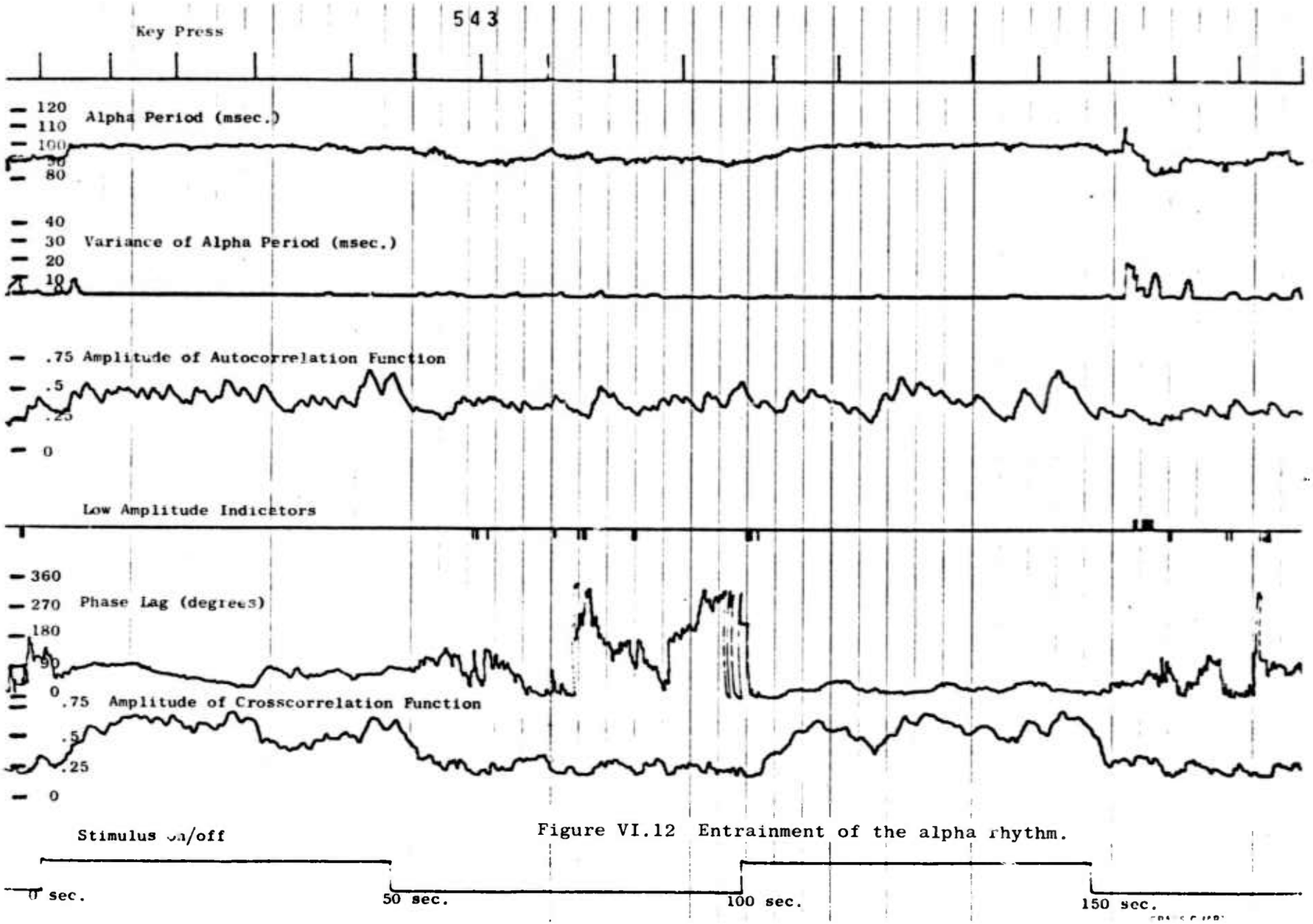

Figure VI.12 Entrainment of the alpha rhythm.

VII. PHASE CONTINGENT AVERAGES

Evoked response averaging is a widely used method for extracting stimulus-coherent signals from random noise. As we suspected the traditional method for averaging conceals other interesting features of the VER which can be preserved through the application of a new method of averaging called phase contingent expansion.

The coincidence between a photic flash stimulus and EEG alpha phase can be expected to be statistically random if the flashes are delivered at arbitrary intervals and if the minimum interval between a single flash or group of flashes is sufficiently long to allow for the complete dissipation of the effects of the previous flash or flashes. Thus, for the traditional visual evoked response, the component sample epochs are initiated with the flash falling with equal probability (equal frequency) on all possible phases of alpha. In other words, the traditional AEP is an average conditional only upon the occurrence of the flash, and assumes that the response looked for in the averaging process is stimulus locked. However, if the cortical response to the flash were also influenced by the phase of the alpha rhythm at the time of the flash, some modification of the averaging technique would be required to bring out the phase contingent properties of the VER.

The phase contingent expansion of the visual evoked response described here is such a method. By regrouping sample epochs of the VER according to the phase of the alpha rhythm at the time of each flash stimulus, a complete series of phase contingent sub-averages containing all component data sample epochs in the VER is obtained. The sub-averages are displayed according to selected flash-phase coincidence ranges in ascending phase order.

Quadrature analysis of the EEG alpha rhythm is accomplished using a somewhat simplified version of a technique described in a previous report. The EEG signals are first band limited (by the transversal filter mentioned in Data Analysis) to include the subject's alpha rhythm. Reference cosine and sine waves using the subject's mean alpha frequency are generated with the condition that for each sample epoch of EEG data, the peak of the cosine wave is always coincident with the stimulus (or trigger) of the sample epoch. Thus, the cosine and sine waves are stimulus-locked coherent rhythms which, by the quadrature technique, will yield the continuous phase relationship, $\phi_Q(\cdot)$, of these waves to the sample epoch in question. The quadrature approach to alpha phase classification is summarized in Figure VII.1.

An example of a phase contingent expansion of a visual average evoked potential is shown in Figure VII.2. In this example, the sample epochs of EEG data were classified into twenty phase ranges covering one complete cylce of the alpha rhythm. The sample epochs in each phase range were then averaged and normalized. The phase contingent averages are arranged in ascending order beginning with the surface negative peak and ending with the next surface negative peak of the alpha cycle. It can be seen that there is a systematic adjustment in each of the contingent averages to achieve a position deflection in the region of the dominant P wave in the grand mean (displayed as a heavier function at the top of the phase contingent series). By comparison of the above series with a similar phase contingent series (Figure VII.3) obtained in the absence of photic stimulation (there was a trigger pulse for the purpose of phase classification but the strobe was inhibited), we see that the greatest phase shifting of the alpha rhythm in response

QUADRATURE CLASSIFICATION OF α PHASE

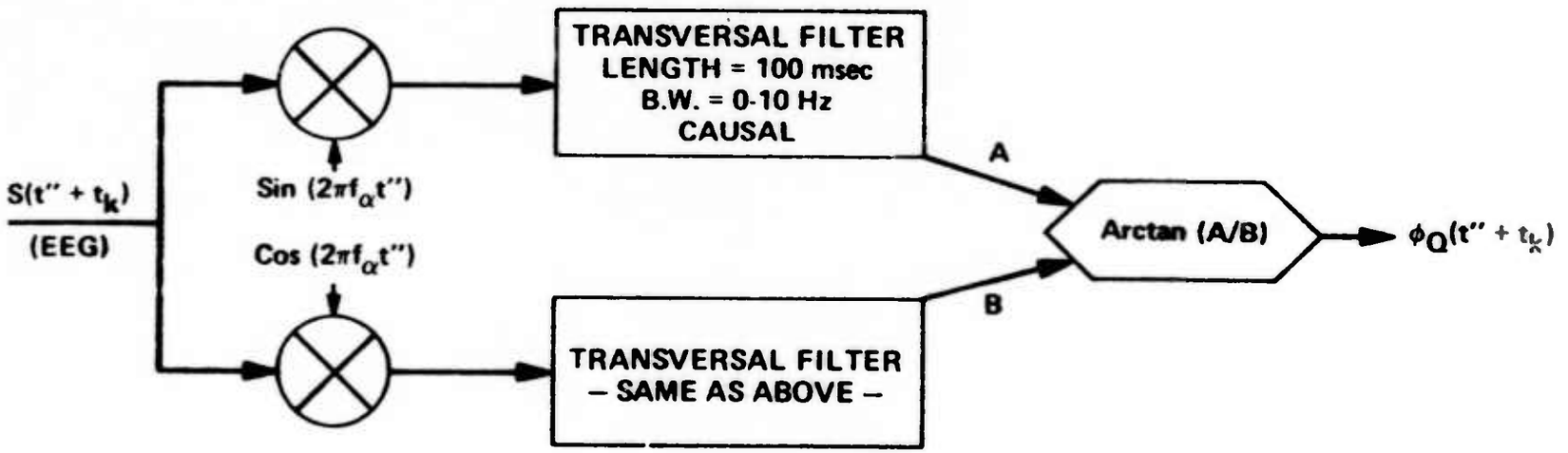

$-100 \text{ msec} \leq t'' < t'_{MAX}$

$f_\alpha \sim 8$ TO 12 Hz

t_k IS THE TIME OF THE k^{th} STIMULUS

Figure VII.1 Application of quadrature to obtain the phase of the EEG, $\{s(t'' + t_k)\}$, of a sample epoch.

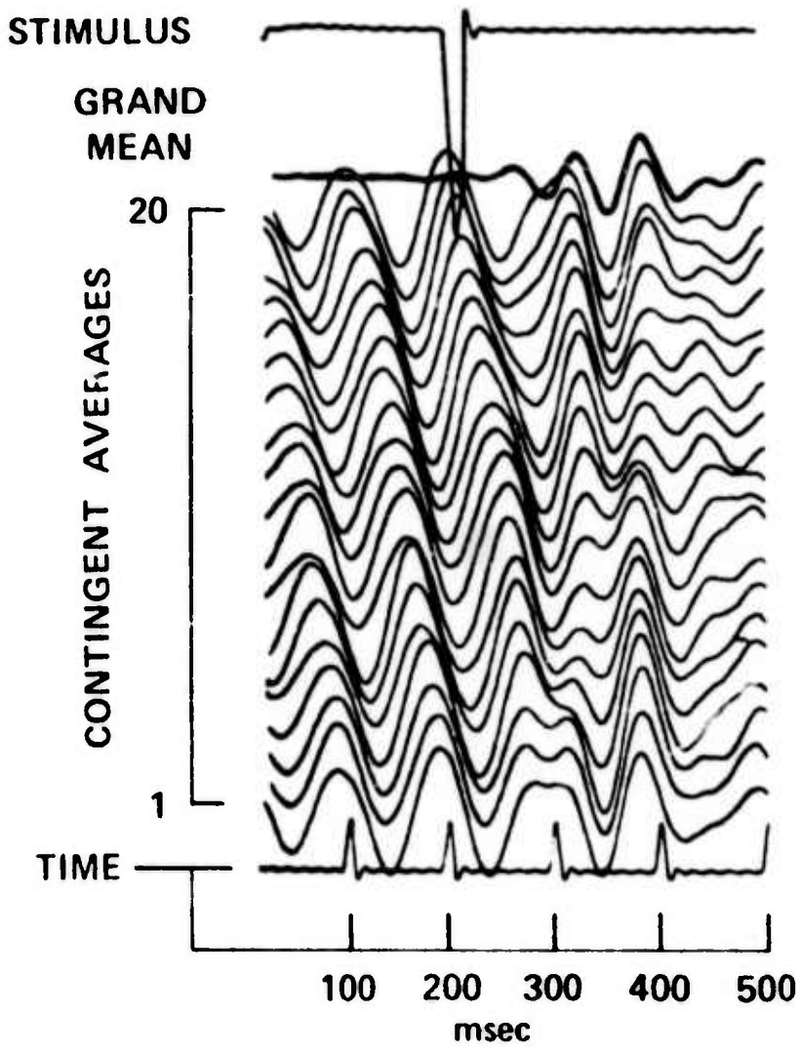

Figure VII.2 Phase contingent averages of visual evoked responses. Each sample epoch was classified with respect to the phase of the alpha rhythm at the moment the flash stimulus was delivered. The "grand mean" is the traditional average of all the epochs without regard to phase.

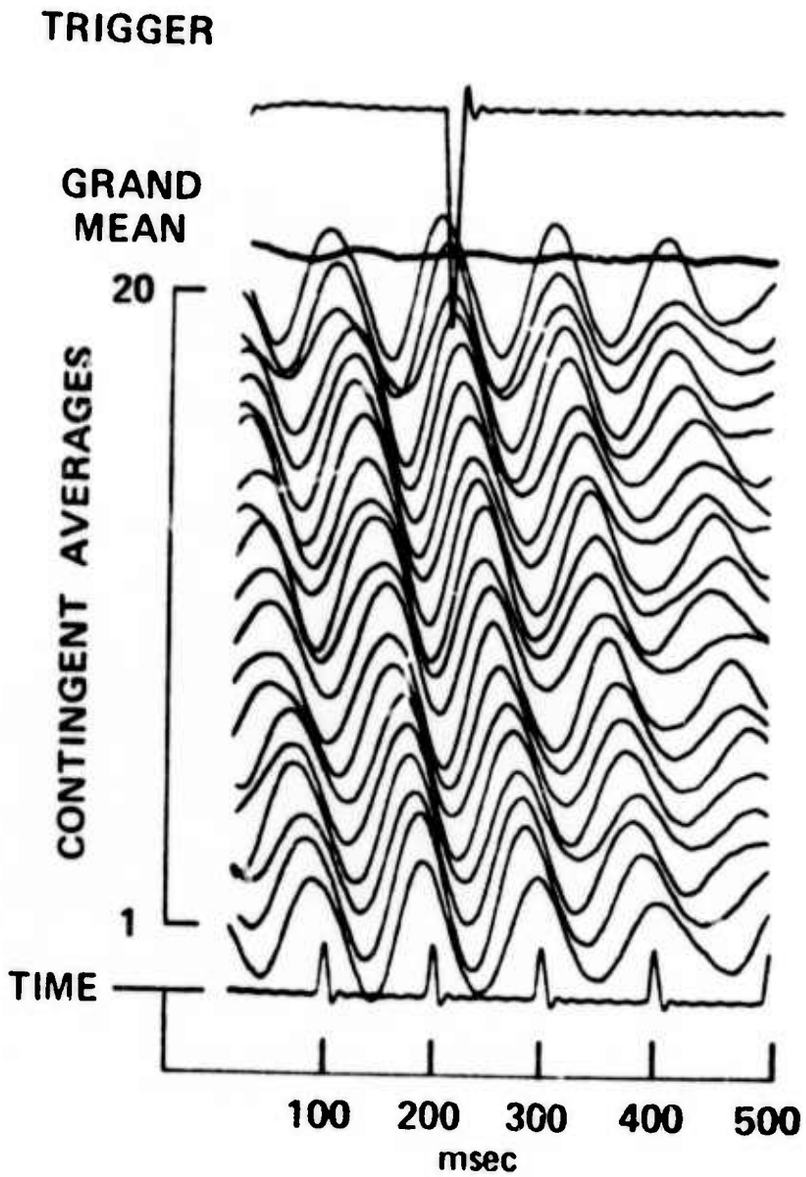

Figure VII.3 Phase contingent averages in the absence of photic stimulation.

The "trigger" simply indicates the basis of phase classification; the strobe was inhibited.

to photic stimulation occurs in the mid-range of the alpha cycle. We are currently studying the signal-to-noise properties of the phase contingent sample epochs in the time region of the dominant P wave. Our preliminary results suggest that the signal-to-noise ratio is the poorest in the mid-range of the alpha cycle where the greatest shifting of the autonomous alpha phase must take place in response to photic stimulation. This agrees with the observation of various investigators that reaction times are longer and sensory thresholds are higher for stimuli delivered at these phase contingencies than for stimuli that are contingent with surface negative peak phases. These studies will be reported in greater detail in a later report.

VIII. CONCLUSION

As described in this report, our work has been proceeding towards the goals that we proposed. We now have better techniques to deal with the errors and distortions of the eye-movement data as measured by the Biometrics Eye-Movement Monitor unit. We believe that we have utilized the Biometrics unit to the best of its capability. Some prediction schemes which predict the eye-fixation points have been implemented and new ones are being developed. A large amount of eye-movement data has been collected and is being analyzed. The analysis will give us a better understanding of the characteristics of the saccadic movement and the fixation. It is expected to lead to better practical predictive models. A new experiment paradigm has been set up for the study of visual scanpaths associated with both superior and inferior imagery. A real-time scanpath analyzer has been developed and implemented. In the offing, we shall see new interesting results in the scanpath study with the aim to find the scanpath which will result in superior memory. We have found a definite excitability cycle correlated with the phase of the alpha rhythm at one instant of photic stimulation via a phase contingent analysis of visual evoked responses. An EEG signal model has been conceived and studied with the hope that it will aid us in building better tracking models for the brain states. We have also, in this period, expanded our computer system to better suit our needs, and completed a computer program dubbed "SEER" that was designed to open up a new avenue for the study of visual scanpaths.

With the continuously up-dated information concerning the eye position and brain state for adjusting the stimulus parameters and the tracking and prediction techniques, we should be able to guide the eyes

to fixate at the optimal locations and at the optimal time instants such that the vividness and persistence of the desired after-images will be enhanced. Future works are planned along the lines to get a better handle of these optimal locations and optimal time instants. Armed with this information, we shall attempt to devise real-time strategies for the control of visual target impression and visual image (memory) persistence and/or recall ability to complete our design of the closely-coupled man-machine system for visual memory tracking and training.

LIST OF PUBLICATIONS

During this reporting period, the following papers have been published/presented/submitted:

1. "A Model for the Photically Stimulated Electroencephalographic Signals", Proceedings of the 12th Annual San Diego Biomedical Symposium, Vol. 12, pp. 5-16, 1973.

2. "The Graphics Software DEC Forgot to Include", Proceedings of the DECUS Spring Symposium, pp. 67-68, 1973.

3. "Real-time EEG Analysis and Monitoring Using In-phase and Quadrature Components", Proceedings of the 26th Annual Conference on Engineering in Medicine and Biology, p. 401, 1973.

4. "Estimating Signal and Noise in Coherent Time Averages of EEG Data", Proceedings of the 26th Annual Conference on Engineering in Medicine and Biology, p. 398, 1973.

5. "Error-free Representation of EEG Signals", Proceedings of the 1973 IEEE International Conference on Systems, Man and Cybernetics, pp. 242-243, 1973.

6. "Phase Contingent Expansion of the Visual Evoked Response (VER)", presented at the 13th Annual San Diego Biomedical Symposium and to be published in the Proceedings, 1974.

7. "Computer Determination of Eye Fixations and Saccades", submitted and accepted for presentation at the 27th Annual Conference on Engineering in Medicine and Biology in October, 1974.